Inflammation increases the penetrance of behavioral impairment in *Shank3* haploinsufficiency mice – can it explain the behavioral regression in Autism?

Authors: Sheng-Nan Qiao, PhD[1], Sung Eun Wang, PhD[1, 6], Kun-Yong Kim, PhD[1], Sungsin Jo, PhD[7], Yong-Hui Jiang, MD, PhD [1-5]

Affiliation: [1]Department of Genetics, [2]Department of Neuroscience, [3]Department of Pediatrics, and [4]Department of Obstetrics, Gynecology & Reproductive Sciences, Yale University School of Medicine, 333 Cedar Street, New Haven, CT 06510 USA

[5]Wu-Tsai Institute, Yale University, 100 College Street, New Haven CT 06520 USA

[6]Department of Systems Biology, Yonsei University, Yonsei-ro 50, Seodaemun-gu, Seoul, South Korea

[7]Department of Biology, Soonchunhyang University, Soonchunhyang-ro 22, Sinchang-myeon, Asan, South Korea

Correspondence:

Yong-Hui Jiang, MD, PhD.

Department of Genetics, Neuroscience, Pediatrics, and OB/Gyn & Reproductive Sciences

TAC S317/S320

Yale University School of Medicine

300 Cedar St, New Haven, CT 06519

Tel: 203-785-2429

Email:yong-hui.jiang@yale.edu

Running title: Neuroinflammation Susceptibility in Autism

Abstract

Behavioral regression occurs in ~40% of *SHANK3*-associated autism spectrum disorder (ASD). We previously reported that significant behavioral regression in a small cohort with *SHANK3* haploinsufficiency patients, triggered by subclinical infections, responded to immunomodulator treatments. We hypothesize that behavioral regression results from the interplay between *SHANK3* deficiency and neuroinflammation. Using *Shank3* exon 4-22 deletion heterozygous mutant (*Sh3*$^{+/-}$) mouse, which shows no significant behavior impairments, we established a preclinical model – *Shank3* haploinsufficiency mouse undergoing systemic inflammation challenge via intraperitoneal injection of lipopolysaccharides (LPS). We found that, two weeks after LPS challenge, wild-type mice (WT) recovered but *Sh3*$^{+/-}$ mice exhibited motor impairment, anxiety-like behaviors, and excessive grooming, similar to *Shank3* exon 4-22 deletion homozygous mutants. Anti-inflammatory treatment partially reversed LPS-induced behavioral changes. Transcriptomic analysis revealed upregulation of neuroinflammation-related genes and downregulation of synaptic function-related genes in *Sh3*$^{+/-}$ mice in response to LPS. Especially, pro-inflammatory genes and microglia markers were overly activated that may result from the increased toll-like receptor 4 (TLR4) in *Sh3*$^{+/-}$ mice. Microglia overactivation elevated synapse engulfment and disrupted synaptic protein may underlie LPS-triggered worsen behavior phenotypes in *Sh3*$^{+/-}$ mice. Our findings indicate that neuroinflammation increases the penetrance of behavioral impairment in *Shank3* haploinsufficiency mice and support a potential mechanism for the behavioral regression in human *SHANK3* disorders for future investigations.

45 **Introduction**

46 Autism spectrum disorder (ASD) is a group of neurodevelopmental conditions with
47 typical onset before the age of three [1]. A significant proportion of children with ASD shows
48 developmental arrest at an early developmental age and behavioral regression
49 throughout the lifespan. Behavioral regression is characterized by loss of previously
50 acquired skills, including loss of purposeful hand use, loss of acquired speech, and gait
51 abnormalities [2-4]. Catatonic features are frequently associated with behavioral regression
52 observed in ASD [5,6]. However, the underlying mechanism for the early developmental
53 arrest and behavioral regression remains poorly understood.

54 The *SHANK3* mutation is one of the most common monogenic defects associated
55 with ASD in humans [7-10]. Genetic mutations in *SHANK3* gene can manifest as Phelan-
56 McDermid Syndrome (PMS), characterized by a chromosomal deletion of 22q13.3 or
57 single nucleotide variants, indels, exonic deletions within the *SHANK3* gene in individuals
58 with primary ASD [11]. Patients with *SHANK3* haploinsufficiency also exhibit severe
59 intellectual disability, motor deficits, and speech delays [12-14]. Developmental regression
60 with catatonic features has been reported in ~40% of cases with *SHANK3*
61 haploinsufficiency [15-20]. We previously described four patients with pathogenic *SHANK3*
62 mutations who experienced acute and severe behavioral regression following possible
63 subclinical viral infections [21]. Notably, treatment with intravenous immunoglobulins (IVIG)
64 combined with anti-inflammatory drugs and immunomodulators significantly reversed the
65 behavioral regression in these cases [21]. This clinical report strongly suggests a potential
66 link between inflammation and behavioral regression associated with *SHANK3*

67 haploinsufficiency. However, the direct causality could not be investigated and determined
68 from human studies.

69 SHANK3 protein is primarily characterized as a scaffold protein located at the
70 postsynaptic density of neurons, interacting with other synaptic proteins and affecting
71 synaptic function [22]. However, the role of SHANK3 in function of non-neuronal cells such
72 as microglia has been poorly studied [23-26]. Microglia activation can sculpt synapses and
73 brain circuits and change animal behavioral phenotypes during normal development as
74 well as in response to neuroinflammation [27,28]. Aberrant microglia activation has been
75 associated with ASD[29-32]. Our previous studies showed that inflammation induces acute
76 behavioral changes [33] and aggravates hypothermia in *Shank3* mutant mouse model [34].
77 These initial findings suggest a potential mechanistic link between *SHANK3* deficiency
78 and inflammatory response.

79 Our lab previously generated a *Shank3* mutant mouse line with a deletion of exon
80 4 to 22 (*Shank3*$^{\Delta e4\text{-}22}$) that disrupts most of the *Shank3* coding region[35]. *Shank3*$^{\Delta e4\text{-}22}$
81 homozygous but not heterozygous mice showed robust face validity for autism-like
82 behaviors[35]. Therefore, *Shank3*$^{\Delta e4\text{-}22}$ heterozygous mice offer a unique opportunity to
83 examine the interaction between genes and environment, specifically whether
84 neuroinflammation may modify the penetrance of behavioral phenotypes associated with
85 *SHANK3* deficiency in humans. In this study, we utilized the *Shank3*$^{\Delta e4\text{-}22}$ heterozygous
86 mice and investigated the behavioral outcome, transcriptomic profiles, microglia
87 activation, and synapse marker after systemic inflammatory challenge induced by
88 lipopolysaccharides (LPS). These findings provide a general insight on the role of
89 neuroinflammation in ASD susceptibility.

Results

Systemic inflammation via LPS modified the penetrance of motor dysfunction, anxiety-like behavior, and repetitive behavior in *Shank3*$^{\Delta e4\text{-}22}$ heterozygous (*Sh3*$^{+/-}$) mice.

To explore whether inflammation plays a role in regression of ASD-associated behaviors, we challenged *Sh3*$^{+/-}$ mice by intraperitoneal injection of LPS (*Sh3*$^{+/-}$+ LPS). Control mice were given the same volume of normal saline (PBS) (*Sh3*$^{+/-}$ + PBS). Both LPS-treated *Sh3*$^{+/-}$ and wild-type (WT) mice experienced weight loss at 24 hours compared to PBS-treated mice (**Fig. 1A**). This indicated systemic inflammation induced by LPS, consistent with previous reports [36]. LPS-treated mice regained body weight at 72 hours post-injection, suggesting recovery from the LPS challenge (**Fig. 1A**). Acute behavioral changes, including decreased locomotor activity [37], social avoidance [38], and depressive-like behavior [39], have been reported in LPS-treated mice around 24 hours post-injection. However, interpretating these behavioral changes in the context of ASD model may be confounded by immediate sickness of test mice [33,40,41]. Therefore, we performed behavioral analysis two weeks after LPS injection to distinguish “LPS and SHANK3 haploinsufficiency interaction effect” vs. “acute LPS effect” (**Fig. 1B**). The *Shank3*$^{\Delta e4\text{-}22}$ homozygous (*Sh3*$^{-/-}$) group was included for a comparison [35].

To assess the motor coordination, latency to fall from the rotarod was measured in both steady speed (16 rpm) and accelerated speed (4-40 rpm) conditions. As expected, *Sh3*$^{-/-}$ mice showed significantly reduced latency to fall compared to WT+PBS group. No significant difference was observed between WT+PBS and WT+LPS groups, but *Sh3*$^{+/-}$ mice treated with LPS showed significantly shorter latency to fall than the PBS group (**Fig.**

113 **1C-D**). The duration of mouse spent in center of open field test (OFT) showed no
114 significant difference between WT+PBS and WT+LPS groups, but *Sh3*$^{+/-}$+LPS spent
115 significantly less time in the center compared to *Sh3*$^{+/-}$+PBS (**Fig. 1E**). In the light/dark
116 box test, distance of mouse moved in light chamber showed no significant difference
117 between WT+PBS and WT+LPS groups while *Sh3*$^{+/-}$+LPS significantly moved less in light
118 chamber compared to *Sh3*$^{+/-}$+PBS (**Fig. 1F**). Repetitive behavior was assayed through
119 scoring grooming behavior. *Sh3*$^{+/-}$+LPS showed significantly longer grooming duration
120 than *Sh3*$^{+/-}$+PBS while WT+PBS and WT+LPS groups were comparable (**Fig. 1G**). We
121 also conducted a three-chamber social preference test. As expected, *Sh3*$^{-/-}$ mice showed
122 no preference for social targets compared to WT. However, both LPS- and PBS-treated
123 *Sh3*$^{+/-}$ and WT mice spent significantly more time in the chamber with the social target (S)
124 or in the proximity region of the social target (SP) (**Fig. 1H-I**).

125 To explore potential sex effect, we compared motor function and sociability in both
126 PBS- and LPS-treated female and male *Sh3*$^{+/-}$ mice. LPS-treated male *Sh3*$^{+/-}$ mice
127 exhibited significant reduced latency to fall in rotarod, although no significant difference
128 found between LPS and PBS group in female *Sh3*$^{+/-}$ mice (**Supplementary Fig. 1A-B**).
129 Both LPS- and PBS-treated male *Sh3*$^{+/-}$ mice spent significantly more time in S or SP, but
130 no significant difference found in female *Sh3*$^{+/-}$mice (**Supplementary Fig. 1C-D**). Taken
131 together, our results indicated that, LPS treatment in *Sh3*$^{+/-}$ mice significantly impaired the
132 motor performance on rotarod, changed exploratory or anxiety-like behaviors in OFT and
133 light/dark box test, and increased grooming duration, but did not affect sociability in three-
134 chamber test. By comparison, LPS treatment in WT mice did not have any significant
135 effect on those behaviors. These findings suggest the interplay of inflammation and

136 *Shank3* haploinsufficiency in select domains of behaviors.

137 To assess whether anti-inflammation treatment can reverse the behavioral
138 changes induced by LPS in *Sh3*$^{+/-}$ mice, we applied mefenamic acid (MFA), a nonsteroidal
139 anti-inflammatory drug (NSAID). One of the MFA targets is the intracellular
140 cyclooxygenase (COX) signaling, which can be activated by LPS [42-44]. Previous study
141 also reported that MFA has neuroprotective effect [45]. Given that both WT+LPS and *Sh3*$^{+/-}$
142 +LPS group exhibited impaired motor function at 1 week after the LPS injection
143 (**Supplementary Fig. 2A-B**) but such behavior deficits of WT+LPS group recovered to
144 baseline at 2-week post-injection (**Fig. 1C-D**), we chose day 7 post-injection as the
145 endpoint of MFA treatment (**Fig. 2A**). We administered MFA via intraperitoneal injection
146 once a day for seven days following LPS injection and then performed rotarod test 24
147 hours after the final dose of MFA to evaluate the treatment efficacy (**Fig. 2A**). In the steady
148 speed (16 rpm) rotarod test, both WT+LPS+MFA and *Sh3*$^{+/-}$+LPS+MFA groups showed
149 significantly increased latency to fall compared to vehicle-treated groups (**Fig. 2B**),
150 suggesting that MFA effectively mitigated the motor function deficits induced by LPS.
151 *Sh3*$^{+/-}$+LPS+MFA showed trend of shorter latency to fall than WT+LPS+MFA (**Fig. 2B**, p
152 = 0.091), suggesting potential less pronounced anti-inflammatory efficacy and the
153 presence of exacerbated inflammatory responses in *Sh3*$^{+/-}$ mice. In contrast, in the
154 accelerated speed (4-40 rpm) rotarod test, MFA did not restore motor function in either
155 WT or *Sh3*$^{+/-}$ mice (**Fig. 2C**). Moreover, when comparing MFA treatment in female and
156 male *Sh3*$^{+/-}$ mice, MFA significantly increased latency to fall in female *Sh3*$^{+/-}$ mice but not
157 in male *Sh3*$^{+/-}$ mice (**Fig. 2D-E**). Overall, our results showed that LPS-induced motor
158 function impairment in *Sh3*$^{+/-}$ mice can be partially reversed by anti-inflammatory

159 treatment. Future studies will include additional behavioral assays, as well as time-course
160 and dose-dependent responses to MFA treatment.

161 **LPS-induced differentially expressed genes (DEGs) were associated with**
162 **neuroinflammation and neurotransmission in *Sh3*$^{+/-}$ mice.**

163 To understand how LPS-induced inflammation modifies the penetrance of motor
164 impairment in *Sh3*$^{+/-}$ mice, we analyzed the transcriptomic profiles in the forebrains by
165 bulk RNA-sequencing (RNA-seq) (**Supplementary Fig. 3A-B, Supplementary Tables 1**
166 **and 2**). LPS treatment induced hundreds of differentially expressed genes (DEGs) in both
167 WT and *Sh3*$^{+/-}$ mice compared to PBS-treated groups. The number of upregulated genes
168 (488 DEGs in *Sh3*$^{+/-}$+LPS vs. *Sh3*$^{+/-}$+PBS and 433 DEGs in WT+LPS vs. WT+PBS) was
169 greater than that of downregulated genes (75 DEGs in *Sh3*$^{+/-}$+LPS vs. *Sh3*$^{+/-}$+PBS and
170 108 DEGs in WT+LPS vs. WT+PBS) (**Fig. 3A-B**). We identified 88 upregulated and 37
171 downregulated DEGs between *Sh3*$^{+/-}$+LPS vs. WT+LPS (**Fig. 3C**). Although we found 67
172 upregulated and 33 downregulated genes when comparing transcriptomic profiles
173 between *Sh3*$^{+/-}$+PBS and WT+PBS (**Fig. 3D**), those genes barely overlapped with any
174 LPS-induced DEGs observed in *Sh3*$^{+/-}$ mice. Next, we compared the overlapping genes
175 among four comparisons (**Fig. 3E-F, Supplementary Tables 3 and 4**). A total of 313
176 shared upregulated and 12 shared downregulated DEGs were identified between
177 WT+LPS vs. WT+PBS and *Sh3*$^{+/-}$+LPS vs. *Sh3*$^{+/-}$+PBS. Those shared DEGs probably
178 represent the LPS-induced neuroinflammatory responses in mouse brains. Eight
179 upregulated genes shared among *Sh3*$^{+/-}$+LPS vs. WT+LPS, *Sh3*$^{+/-}$+LPS vs. *Sh3*$^{+/-}$+PBS
180 and WT+LPS vs. WT+PBS were well-known for their roles in neuroinflammation (**Fig. 3E**
181 highlighted with white underline, **Table 1**). Interestingly, 10 upregulated genes and 5

182 downregulated genes were found only in *Sh3*$^{+/-}$ mice not in WT mice in response to LPS
183 (**Fig. 3E-F** highlighted with green underline, **Table 2-3**), suggesting that LPS-induced
184 neuroinflammation in *Sh3*$^{+/-}$ mice is mediated by distinct signaling pathways. Additionally,
185 when we compared the overlapping genes between *Sh3*$^{+/-}$+PBS vs. WT+PBS and *Sh3*$^{+/-}$
186 +LPS vs. WT+LPS, only 4 genes in total (two are protein-coding genes) were identified
187 (**Fig. 3E-F** highlighted with red underline). Particularly, *Acr* is a *Shank3* subordinate
188 adjacent gene, whose expression increased when *Shank3* is deleted [46]. To further
189 characterize the function of DEGs from RNA-seq, we performed the pathway analysis
190 using the QIAGEN Ingenuity Pathway Analysis (IPA) [47]. We identified more activated
191 inflammation-associated pathways in response to LPS challenges in both *Sh3*$^{+/-}$ and WT
192 (**Supplementary Fig. 4 and 5**). In contrast, inhibited neurotransmission-related pathways
193 including NMDA receptor and calcium signaling pathways were only observed in LPS-
194 treated *Sh3*$^{+/-}$ but not in LPS-treated WT (**Supplementary Fig. 4 and 5**). To understand
195 the distinct molecular pathways in LPS-treated *Sh3*$^{+/-}$ mice, we delved into the pathway
196 analysis from *Sh3*$^{+/-}$+LPS vs. WT+LPS (**Supplementary Fig. 6**). The top five activated
197 pathways were all related to inflammatory processes. The top two inhibited pathways,
198 cardiac conduction and CREB signaling in neurons, represent inhibited neuron signal
199 transmission and neuronal functions. The other three inhibited pathways, HIF1α signaling,
200 eNOS signaling and phagosome formation pathways, represent increased neuronal
201 vulnerability to stress and inflammatory stimuli. In addition to the top five pathways with
202 highest z score value, we noticed that most of the upregulated signaling pathways in
203 response to LPS were all inflammation-related, including cytokine storm pathway and
204 neuroinflammation pathway (**Fig. 3G**). In contrast, the downregulated pathways in LPS-

205 treated *Sh3*$^{+/-}$ mice were neuronal and synaptic function-related, including potassium
206 channel pathway, glutamatergic signaling pathway, acetylcholine signaling pathway, and
207 gap junction signaling pathway (**Fig. 3G**). Overall, our RNA-seq results suggested that a
208 combination of exacerbated neuroinflammatory responses and impaired neuronal
209 functions is attributed to the LPS-induced behavioral regression in *Sh3*$^{+/-}$ mice.

210 **Neuroinflammation was increased in *Sh3*$^{+/-}$ mice**

211 To investigate how LPS leads to aggravated neuroinflammation in *Sh3*$^{+/-}$ brains,
212 we first measured the RNA expression of the pro-inflammatory cytokines *Il1b* and
213 chemokines *Cxcl10* using RT-qPCR. *Il1b* and *Cxcl10* have been identified as common
214 upregulated genes across all LPS-treated groups in RNA-seq (**Table 1**). RT-qPCR
215 confirmed that LPS significantly increased *Il1b* and *Cxcl10* expression in both WT and
216 *Sh3*$^{+/-}$ mice compared to PBS groups. Although no significant difference in *Il1b* and *Cxcl10*
217 expression was found between *Sh3*$^{+/-}$+PBS vs. WT+PBS, *Sh3*$^{+/-}$+LPS showed
218 significantly increased expression compared to WT+LPS group (**Fig. 4A-B**). A previous
219 study showed that LPS treatment upregulates microglia marker gene *Cx3cr1* while
220 downregulates microglia homeostasis gene *P2ry12* expression [48]. Therefore, we
221 examined the expression of microglia markers *Cx3cr1* and *P2ry12* using RT-qPCR. We
222 found that, as expected, LPS significantly increased *Cx3cr1* expression and decreased
223 *P2ry12* expression in both WT and *Sh3*$^{+/-}$ mice compared to PBS groups (**Fig. 4C-D**).
224 However, *Cx3cr1* expression was comparable between *Sh3*$^{+/-}$+PBS and WT+PBS but
225 significantly increased in *Sh3*$^{+/-}$+LPS compared to WT+LPS group (**Fig. 4C**). In contrast,
226 *P2ry12* expression was significantly higher in *Sh3*$^{+/-}$+PBS than in WT+PBS and higher in

227 *Sh3*$^{+/-}$+LPS than in WT+LPS (**Fig. 4D**).

228 We further examined microglia activation by examining the expression of IBA-1, a
229 marker widely used for the assessment of microglia activation state [49] (**Fig. 4E-F**).
230 Compared to PBS treatment, LPS increased IBA-1 staining intensity significantly at 3
231 hours and 24 hours after LPS treatment in both WT and *Sh3*$^{+/-}$ mice. However, *Sh3*$^{+/-}$
232 +LPS showed significantly higher microglia activation than WT+LPS group at 24 hours
233 but not at 3 hours post-injection. These results indicated that the prolonged activation of
234 microglia contributed to increase of neuroinflammatory responses in *Sh3*$^{+/-}$ mice.

235 Next, to understand the mechanism underlying the LPS-induced microglia
236 overactivation in *Sh3*$^{+/-}$ mice, we analyzed the LPS binding receptor toll-like receptor-4
237 (TLR-4) expression in WT+LPS and *Sh3*$^{+/-}$+LPS groups at 24 hours post-injection [50]. We
238 found that TLR4 expression was significantly higher in *Sh3*$^{+/-}$ than WT with either PBS or
239 LPS treatment (**Fig. 4G-H**). Additionally, we measured the SHANK3 protein expression
240 and found that either PBS- or LPS-treated *Sh3*$^{+/-}$ groups showed a reduction in SHANK3
241 protein expression compared to WT groups as expected, but no changes in SHANK3
242 expression were observed after LPS treatment (**Fig. 4G, I**). TLR4 is known to associate
243 with LPS-induced microglia activation[51-54]. To investigate whether observed TLR4
244 augmentation directly facilitates microglia overactivation in LPS treated *Sh3*$^{+/-}$ mice, we
245 analyzed colocalization between TLR4 and IBA1 (**Fig. 4J-P**). We found that TLR4 and
246 IBA1 expression were well-colocalized in WT, but a small fraction of TLR4 signals in *Sh3*$^{+/-}$
247 mice were not colocalized with IBA1 (**Fig 4J-K**). Although colocalization Pearson's
248 coefficient was similar between WT+LPS and *Sh3*$^{+/-}$+LPS group, colocalization coefficient
249 normalized by TLR4 was lower in *Sh3*$^{+/-}$ mice and the colocalization coefficient normalized

250 by IBA1 was similar (**Fig. 4L-N**). Interestingly, cellular immunofluorescence intensity of
251 TLR4 in *Sh3*$^{+/-}$ mice is slightly lower than WT (**Fig. 4P**). In addition, cellular
252 immunofluorescence intensity of IBA1 was significantly higher in *Sh3*$^{+/-}$ brains (**Fig. 4O**).
253 Given that TLR4 was expressed in many different cell types including astrocytes,
254 neutrophils, and brain endothelial cells [55,56], these findings suggested that elevated TLR4
255 expression in other cell types might contribute to microglia activation in *Sh3*$^{+/-}$ mice.

256 **Microglia activation affected synaptic structure in *Sh3*$^{+/-}$ mice**

257 To uncover how microglia overactivation leads to behavioral changes in *Sh3*$^{+/-}$ mice,
258 we examined microglia engulfment and synaptic structures. We compared lysosome
259 engulfment (lysosome marker CD68 occupancy) and synapse engulfment (presynaptic
260 marker vGluT1 occupancy) between WT+LPS and *Sh3*$^{+/-}$+LPS brains at 24 hours post-
261 injection. While CD68 occupancy was comparable between the two groups, vGluT1
262 occupancy — both within CD68-positive lysosomal puncta in microglia (CD68^{+}IBA1^{+}) and
263 within the microglial cytoplasm (IBA1^{+}) — was significantly higher in *Sh3*$^{+/-}$ mice
264 compared to WT mice (**Fig. 5A-D**). These findings suggest that microglial activation is
265 associated with increased phagocytosis of synaptic materials in the *Sh3*$^{+/-}$+LPS group.

266 To determine whether increased synaptic engulfment leads to synapse dismantling
267 in the *Sh3*$^{+/-}$ brain, we examined the colocalization of the presynaptic marker vGluT1 with
268 the postsynaptic density marker PSD95 at 24 hours following LPS injection. In WT mice,
269 vGluT1 and PSD95 puncta were well colocalized (**Fig. 5E**, arrowhead). In contrast, *Sh3*$^{+/-}$
270 mice displayed discrete PSD95 clusters that did not colocalize with vGluT1 puncta (**Fig.
271 5E**, arrow). Quantitative analysis revealed that the *Sh3*$^{+/-}$+LPS group showed a
272 significantly lower Pearson's correlation coefficient for colocalization, a reduced

273 colocalization coefficient normalized by PSD95, and decreased overall synaptic puncta
274 density compared to the WT+LPS group (**Fig. 5F-H**).

275 Next, we compared the colocalization of vGluT1 and PSD95 among four groups
276 — WT+PBS, WT+LPS, *Sh3*$^{+/-}$+PBS, and *Sh3*$^{+/-}$+LPS — at two weeks after injection. In
277 both WT+PBS and WT+LPS groups, vGluT1 and PSD95 puncta remained closely aligned
278 (**Fig. 5I**). The *Sh3*$^{+/-}$+PBS group also exhibited substantial colocalization of vGluT1 and
279 PSD95; however, some displaced PSD95 fragments were observed, which became more
280 pronounced in the *Sh3*$^{+/-}$+LPS group (**Fig. 5J,** arrow). Consistent with the findings at 24
281 hours post-injection, the *Sh3*$^{+/-}$+LPS group showed a significantly lower Pearson's
282 correlation coefficient for colocalization, a reduced colocalization coefficient normalized
283 by PSD95, and decreased synapse density compared to the other groups (**Fig. 5K-M**).
284 These results support the conclusion that microglial overactivation enhances synapse
285 engulfment and contributes to synaptic structure disorganization in *Sh3*$^{+/-}$ mice in
286 response to LPS-induced inflammation.

287 To investigate whether disrupted synaptic structure caused PSD protein reduction
288 and synaptic dysfunction in *Sh3*$^{+/-}$ mice, we explored excitatory postsynaptic scaffold
289 proteins PSD95 and HOMER 1b/c expression (**Fig. 5N**). No significant change of PSD95
290 was observed between *Sh3*$^{+/-}$+PBS vs. WT+PBS. However, PSD95 was significantly
291 decreased in the *Sh3*$^{+/-}$+LPS compared to both the WT+LPS group (~28% reduction) and
292 the *Sh3*$^{+/-}$+PBS group (~17% reduction), suggesting that LPS treatment reduced the
293 PSD95 protein level in *Sh3*$^{+/-}$ mice not in WT mice (**Fig. 5O**). In contrast, HOMER 1b/c
294 expression was significantly decreased in *Sh3*$^{+/-}$+PBS vs. WT+PBS (~41% reduction) and
295 in *Sh3*$^{+/-}$+LPS vs. WT+LPS (~23% reduction) but showed no significant change between

296 *Sh3*$^{+/-}$+LPS vs. *Sh3*$^{+/-}$+PBS. It indicated that LPS treatment did not further reduce
297 HOMER expression (**Fig. 5P**). PSD95 is critical for excitatory synapse function through
298 its interactions with NMDA and AMPA receptors[57]. We examined whether the change of
299 PSD95 may lead to the change of the expression of major subunits of NMDA receptor
300 subunit NR2A and the AMPA receptor subunit GluA1 associated with LPS treatment (**Fig.**
301 **5Q**). We found that NR2A expression was reduced in the *Sh3*$^{+/-}$+LPS group compared to
302 both the WT+LPS group and the *Sh3*$^{+/-}$+PBS group (**Fig. 5R**). The GluA1 expression was
303 significantly reduced in *Sh3*$^{+/-}$+LPS mice compared to both the WT+LPS group and
304 *Sh3*$^{+/-}$+PBS group **(Fig. 5S**). Taken together, these results suggested a mechanistic
305 convergence between LPS-induced neuroimmune responses, and the synaptic
306 disruptions known to arise from Shank3 deficiency.

Table 1. Eight Upregulated DEGs shared among *Sh3*$^{+/-}$+LPS vs. WT+LPS, *Sh3*$^{+/-}$+LPS vs. *Sh3*$^{+/-}$+PBS and WT+LPS vs. WT+PBS.

Gene name	Protein function
Bcl3	BCL3 is an autonomous determinant of memory/terminal effector cell balance during CD8^{+} T cell differentiation in response to acute viral infection [58].
Ccl3	CCL3 as a cytokine contributes to progressive tissue damage and functional impairment during secondary injury after spinal cord injury [59].
Cxcl10	CXCL10 as a lymphocyte chemoattractant contributes to the intraparenchymal trafficking of lymphocytes during acute CNS inflammation [60].
Gbp5	GBP5 as a GTPase participates in the regulation of immunity and neuroinflammation [61].
Ifitm6	IFITM6 encodes cell surface proteins that modulate cell-cell adhesion and cell differentiation, is induced in various macrophages, and increases expression 24 hours after LPS [62].
Il1b	IL-1β can be acutely induced in the brain following peripheral bacterial infections, and microglia facilitate exaggerated IL-1β production upon exposure to acute systemic inflammation induced by bacterial LPS [63].
Steap4	STEAP4 as a key effector molecule contributes to the pathogenesis of neuroinflammation in experimental autoimmune encephalomyelitis [64].
Tlr2	Toll-like receptors (TLRs) are fundamental sensor molecules of the host innate immune system, which detect conserved molecular signatures of a wide range of microbial pathogens and initiate innate immune responses via distinct signaling pathways [65].

307

Table 2. Ten upregulated DEGs only shared between *Sh3*$^{+/-}$+LPS vs. WT+LPS and *Sh3*$^{+/-}$+LPS vs. *Sh3*$^{+/-}$+PBS, not include in WT+LPS vs. WT+PBS.

Gene name	Protein function
Alms1-ps1	ALMS1, centrosome and basal body associated, pseudogene 1.
Atf3	ATF3 as a transcription factor responds to and exert dual effects on inflammatory responses and in involved in neuroinflammatory response [66].
Ccl12	CCL12 as a chemokine expressed by microglia is involved in inflammation [67].
Fas	Fas/FasL pathway plays a key role in immune homeostasis and leads to excessive neuroinflammation during excessive neuroinflammation [68].
Gm11681	long non-coding RNA.
Hspa1a	HSPA1A and HSPA1B are two subtypes of HSPA1 proteins. HSPA1 is a member of the stress-inducible 70-kDa heat shock protein (HSP70) family, which plays a critical role in the cellular stress response [69,70].
Hspa1b	
Hspb1	
Oas1g	OAS1G is an important murine antiviral response factor, function through activating RNase L to degrade viral RNA in turn inhibiting viral replication and propagation [71].
Prok2	PROK2 is a secreted protein involved in the pathogenesis of several acute and chronic neurological diseases. It shows that PROK2 mediates neuronal cell deaths in traumatic brain injury via ferroptosis [72].

308

Table 3. Five downregulated DEGs only shared between *Sh3*$^{+/-}$+LPS vs. WT+LPS and *Sh3*$^{+/-}$+LPS vs. *Sh3*$^{+/-}$+PBS, not include in WT+LPS vs. WT+PBS.

Gene name	Protein function
4930415F15Rik	SPMIP7 protein is mainly involved in spermatogenesis but is also expressed in the brain and its function is unclear.
AC173482.5	Predicted gene, Gm47797
Gm14393	Predicted gene
Gm5111	Predicted gene
Tgif2	TGIF2 is a transcriptional repressor. Downregulation of TGIF2 is correlated with neuronal apoptosis and development of autism in mice [73].

309

310 **Discussion**

311 In this study, we successfully established a preclinical model and experimental
312 protocol to assess the role of neuroinflammation induced by LPS in *Sh3*$^{+/-}$ mice (**Fig. 6**).
313 We demonstrated that LPS challenge modified the penetrance of motor function deficits,
314 anxiety-like behavior, and repetitive behavior but did not alter social preference in *Sh3*$^{+/-}$
315 mice. More interestingly, the motor and emotion specific behavioral changes are
316 reminiscent of catatonia features that are often observed in humans with *SHANK3*
317 deficiency and idiopathic ASD [74-76]. Additionally, our extensive comparative transcriptome
318 analysis among the different groups validated the experimental protocol of LPS induction
319 and revealed distinct underlying molecular mechanisms. The significantly upregulated
320 genes ubiquitously associated with inflammatory pathways in LPS treated groups
321 indicated the effectiveness of LPS induction. The downregulated genes in multiple
322 pathways associated with neuronal and synaptic functions strongly support a potential
323 causal link between LPS treatment and increased penetrance of abnormal behaviors in
324 *Sh3*$^{+/-}$ mice. Moreover, increased microglia activation and reduced synaptic function from
325 LPS treatment were further validated by molecular experiments. Finally, the partial
326 reversal of motor impairment in LPS treated *Sh3*$^{+/-}$ mice through the anti-inflammation
327 treatment with MFA further supports this causality. Notably, MFA treatment did not restore
328 LPS-treated WT and *Sh3*$^{+/-}$ mice performance in the accelerating speed rotarod. These
329 findings suggest that the mechanisms underlying inflammation-induced motor impairment
330 are different between steady speed and accelerating speed rotarod tests [77]. Additionally,
331 one-week MFA treatment was more effective in female *Sh3*$^{+/-}$ mice than male mice (**Fig.
332 2D-E**) and LPS-treated male *Sh3*$^{+/-}$ mice performance was worse than female ones

333 (**Supplementary Fig. 1A-B**), indicating potential sex difference in motor function[78] and
334 neuroinflammation process[79].

335 The behavior impairments induced by LPS in *Sh3*$^{+/-}$ mice could attribute to the
336 dysfunction of neuronal cells resulted from neuroinflammation. In the previous study that
337 our lab contributed, LPS challenge increased the excitability in D1 but not D2 medium
338 spiny neurons using whole-cell patch clamp recordings and decreased neuron calcium
339 transients in nucleus accumbens in response to social stimuli using *in vivo* Ca^{2+} imaging[33].
340 Our data showed that increased neuroinflammation downregulated genes associated
341 with neuronal and synaptic functions in *Sh3*$^{+/-}$ mice compared to WT mice and reduced
342 synaptic protein PSD95 in *Sh3*$^{+/-}$ mice.

343 LPS-induced neuroinflammation could also alter the function of non-neuronal cells
344 in *Sh3*$^{+/-}$ mice. Our findings of augmented TLR4 expression and microglia activation
345 associated with LPS treatment suggested that microglia are primarily involved in more
346 significant neuroinflammatory responses in *Sh3*$^{+/-}$ mice. Consistent with the findings in
347 many reports in literature supporting that TLR4 mediates microglial activation in brains [51-
348 54], our findings also support that the upregulation of TLR4 contributes to the observed
349 microglial activation following LPS administration. The direct causality between
350 upregulation of TLR4 and microglia activation due to LPS induction has been
351 demonstrated in a recent study[80]. Our observations are consistent with this finding and
352 support the augmented TLR4 as the cause of microglia activation in SHANK3 deficiency
353 mice. Further analysis of TLR4 and IBA1 cellular colocalization indicated that additional
354 cell types might also be involved in LPS-TLR4 (ligand-receptor) mediated
355 neuroinflammation. Cellular fluorescence intensity of TLR4 in fixed brain cortex regions

356 decreased while total protein level of TLR4 in freshly prepared forebrain tissue increased
357 in *Sh3*$^{+/-}$ mice than WT. This inconsistence implied that changes of TLR4 in *Sh3*$^{+/-}$ might
358 be brain region specific and cell type specific, which warranted a future study on the TLR4
359 transduction signaling pathways in *Shank3* haploinsufficiency mouse model.

360 Moreover, we uncovered a mechanistic convergence between LPS-induced
361 neuroimmune responses, and the synaptic disruptions known to arise from Shank3
362 deficiency. We discovered increased microglia engulfment and disrupted synaptic
363 structure in *Sh3*$^{+/-}$ mice. Such dysfunction sustained until 2 weeks later when we identified
364 LPS-triggered behavioral changes only in *Sh3*$^{+/-}$ mice instead of WT mice. Moreover, in a
365 previous study, we reported that the scaffold protein PSD95 expression did not change
366 significantly while HOMER1b/c was significantly reduced in *Sh3*$^{+/–}$ mice[35]. In the current
367 study, we replicated the finding that HOMER1b/c expression is significantly decreased in
368 *Sh3*$^{+/–}$ mice. However, LPS treatment did not further reduce HOMER levels. We also
369 replicated the finding that PSD95 is not changed in *Sh3*$^{+/–}$ mice. However, LPS treatment
370 significantly reduced PSD95 expression in *Sh3*$^{+/–}$ mice not WT mice. This pattern of
371 PSD95 changes in response to LPS, influenced by Shank3 haploinsufficiency, differs from
372 that observed for HOMER1b/c. Although we previously reported no change of NR2A or
373 GluA1 in *Sh3*$^{+/-}$ mice[35], we found that LPS treatment reduced NR2A and GluA1
374 expression in *Sh3*$^{+/-}$ mice instead of WT mice.

375 Our findings represent a first step toward understanding how Shank3
376 haploinsufficiency is linked to neuroimmune signaling. Our previous study showed that
377 SHANK3 deficiency in periphery nerve system contributes to the exaggerated
378 inflammatory responses[81]. Our recently published collaborative study has shown that

379 conditional knock-out of SHANK3 major isoform in brain endothelial cells recapitulated
380 social behavior impairment and other synaptic phenotypes [82]. Our findings are aligned
381 with previous studies showing that *Shank3* deficiency exacerbates the inflammatory
382 responses in peripheral neurons either induced by LPS [34,81] or by maternal immune
383 activation during the pregnancy [83]. Overall, our findings showed that LPS exacerbated
384 neuroinflammation in *Sh3*$^{+/-}$ mouse brains through unique molecular mechanisms as
385 summarized in **Fig. 6** for further investigations in future.

386 In humans, haploinsufficiency of *SHANK3* is highly penetrant for
387 neurodevelopmental impairments [84]. Approximately ~70% of PMS and *SHANK3*
388 deficiency patients met the diagnostic criteria for ASD. The comorbidity of intellectual
389 disability, anxiety, and epilepsy are highly penetrant or common [75]. There is an increasing
390 recognition of behavioral regression and catatonia among young teens with *SHANK3*
391 deficiency [74]. However, the triggers and mechanisms underlying the behavioral
392 regression are largely unknown. Although few clinical case reports implicated
393 neuroinflammation as a trigger [21,85], our findings may offer a mechanistic explanation for
394 the behavioral regressions observed in *SHANK3* patients after experiencing a subclinical
395 infection responded to the immune modulator treatment. Our study may support a link
396 between neuroinflammation and autism susceptibility in general.

397 Our results establish an important proof-of-concept study to dissect the link
398 between neuroinflammation and autism susceptibility. The apparent limitations of our
399 studies include that we have not provided definitive causality for the cell types and specific
400 molecular mechanism directly implicated in the increased neuroinflammatory responses
401 indued by LPS in SHANK3 haploinsufficiency mice. Future studies are warranted to

402 examine dosage- or treatment duration-dependent effects of LPS on behavioral outcomes
403 at different neurodevelopmental stages and in different sexes of *Shank3* deficiency mice.
404 Despite these limitations, our results suggest that *Shank3* haploinsufficiency increases
405 susceptibility to neuroinflammation-induced behavior impairment through distinct
406 molecular pathways. These findings provide new insights into the role of
407 neuroinflammation in ASD and for developing anti-inflammatory treatments as both
408 preventive and therapeutic strategies for behavior regression in ASD that are warranted
409 for further investigations.

410 **Materials and methods**

411 **Animals**

412 Animals were housed under standard 12 h/12 h light/dark cycles (7 AM-7 PM) with
413 food, water ad libitum, controlled temperature and humidity in the Yale University animal
414 facility. Experiments procedures conducted were following the Institutional Animal Care
415 and Use Committee (IACUC) protocol at Yale University (protocol No. 2025-20271).
416 *Shank3*$^{\Delta e4\text{-}22}$ mouse line (Jax Strain #:039524) was generated in-house and had been
417 crossed with C57BL/6J mouse line (Jax Strain #:000664) over 20 generations. Wild-type
418 (*WT*), *Shank3*$^{\Delta e4\text{-}22}$ homozygous (*Sh3*$^{-/-}$) and *Shank3*$^{\Delta e4\text{-}22}$ heterozygous mice (*Sh3*$^{+/-}$)
419 were obtained through heterozygotes breeding as previously described [35]. All experiment
420 procedures were performed within a time frame of 9 AM-5 PM. Animals of the same sex
421 were group housed (2-5 mice per cage). Both male and female mice were used. One
422 cage of mice with same genotype and same sex were assigned to PBS or LPS group
423 randomly. Experimental order of different group was randomized. Mice from multiple
424 groups for same experiments were carried out at same time. Before experiments, each
425 mouse was cataloged with identification number in an excel sheet which included detailed
426 information such as genotype and drug treatment. During experiments, experimenter
427 handled mice based on its identification number and attempted to be semi-blinded. Post-
428 processing, data handling and statistical analysis were semi-automated performed using
429 software stated below. Mice with health problems such as runt, fight wounds,
430 malocclusion, and eye problems, were excluded from experiments. For RNA and protein
431 extraction, mice were deeply anesthetized with 5% isoflurane, then mouse brains were
432 quickly collected, flash frozen in liquid nitrogen and stored in -80 °C freezer until further

433 use. The number of animals used in each experiment was determined based on our lab
434 prior experience and a prior power analysis was calculated using G*power statistics
435 software[86] (**Supplementary table 5**). Total number of mice used for each experiment was
436 as follows: 86 mice for MFA treatment rotarod test, 52-95 mice for open field, rotarod and
437 three-chamber behavior test, 49-66 mice for light/dark box and grooming behavior test,
438 15 mice for RNA sequencing, 40 mice for quantitative PCR, 24 mice for wide-field IBA1
439 staining, 6 mice for TLR4/IBA1 co-staining, 6 mice for microglia engulfment and
440 vGluT1/PSD95 staining at 24 hours post-injection, 12 mice for vGluT1/PSD95 staining at
441 24 hours post-injection, 18 mice for whole-cell protein analysis and 24 mice for synaptic
442 protein analysis. All experiments were replicated at least once, except that RNA
443 sequencing was done one time.

444 **Drug**

445 Three to five-week-old female and male mice were intraperitoneally injected with
446 LPS (Sigma, L6511) in saline at 1 mg/kg or same volume of saline (PBS). To test the
447 mefenamic acid (MFA) anti-inflammatory effect on behavior improvement, MFA
448 (Thermofisher, AAJ6270522) dissolved in DMSO at 5 mg/kg or the same volume of
449 DMSO (vehicle) was injected intraperitoneally to the mice with LPS injection once a day
450 for 7 days. Before injection, freshly made stock solution of MFA in DMSO (MFA treatment)
451 or DMSO (vehicle treatment) was diluted with 1:100 ratio in PBS to minimize DMSO
452 toxicity.

453 **Behavior assay**

454 For behavioral experiments, mice were handled for 3 days and habituated in the
455 procedure room for 1 hour before behavioral assays. All behavioral tests were conducted
456 once for each mouse.

457 Anxiety-like behaviors were tested by open field test (OFT) and light/dark box test
458 followed previous studies[35,87]. In OFT, mouse spontaneous activity in Noldus Open Field
459 (4 chambers, 40 (L) x 40 (W) x 30 (H) cm per chamber) over 10 minutes was recorded
460 with EthoVision XT video tracking software (Noldus). The Noldus two-chambered
461 light/dark box is equipped with the lid of dark chamber made by infrared translucent
462 material. The dimensions of the compartment are one third for the dark chamber (20 (L)
463 x 20 (W) x 20 (H) cm) and two thirds for the light chamber (20 (L) x 40 (W) x 20 (H) cm).
464 Mice were firstly placed into the open-light chamber (~700 lux) and given 5 min to freely
465 explore both light and dark (0 lux) chambers. The video was recorded with EthoVision XT
466 video tracking software. Ethovision software was used to automatically score the travel
467 distance and duration in arena.

468 Repetitive behavior was tested by evaluating mouse grooming behaviors. Mouse
469 was placed in a Noldus phenotyper (30 (L) x 30 (W) x 45 (H) cm) and recorded with
470 EthoVision XT video tracking software. Mouse freely explored for 10 minutes and last 5
471 minutes of grooming behavior was hand scored.

472 Motor coordination was tested by rotarod (Med Associate) performance as
473 described [35,88]. Mice were tested in two 5 min trials with an inter-trial interval of 30 min. In
474 accelerating session, revolutions per minute (rpm) of the turning barrel is accelerating
475 from 4 to 40. In steady speed session, the rpm of the turning barrel is fixed at 16. Latency
476 to fall, or to rotate off the top of the turning barrel, was measured by the timer.

477 Social preference was tested by a three-chamber assay as described[88]. An
478 unfamiliar age- and sex-matched mouse was used as a social stimuli mouse in the three-
479 chamber test and habituated under a wired enclosure for 3 days before testing. A
480 customized chamber composed of a rectangular Plexiglas arena (42 (L) x 56.5(W) x 35.8
481 (H) cm) divided into three chambers (each chamber 18.5 x 42 cm), with 2 doors
482 connecting chambers and two enclosures (wired pencil cups with metal vertical bars)
483 located in the two outer chambers. Briefly, the test mouse was habituated in the center
484 chamber for 5 min. Then the social stimuli mouse was placed under one of the pencil
485 cups and 2 doors were lifted allowing the experimental mouse to freely explore the whole
486 arena. The location of the empty and mouse enclosures, and the social stimuli mouse
487 were changed and counterbalanced for each trial. The EthoVision XT video tracking
488 software was used to score the duration of mouse spending in the empty chamber, the
489 mouse chamber, proximity regions (5 cm in distance) close to the empty enclosure, and
490 proximity regions close to the mouse enclosure.

491 **Bulk RNA sequencing**

492 Total RNA was isolated from the forebrain hemisphere using Trizol (Invitrogen,
493 15596018) followed manufacturer protocol and then treated with DNase I (Invitrogen,
494 AM1907) to remove contaminating DNA. RNA samples were sent to Yale Center for
495 Genome Analysis (YCGA) for bulk RNA sequencing (RNA-seq). See details about
496 sequencing process in Supplementary Information. After obtaining the data, low quality
497 reads were trimmed, and adaptor contamination were removed using Trim Galore (v0.5.0).
498 Trimmed reads were mapped to the mouse reference genome (mm10) using HISAT2
499 (v2.1.0) [89]. Gene expression levels were quantified using StringTie (v1.3.3b) [90].

500 Differentially expressed genes were identified using DESeq2 (v 1.22.1) [91]. Unpaired *t*-test
501 *p* value was used for filtering DEGs with significant differences between the two groups.
502 Log_2fold cutoff threshold at 1 and $p < 0.05$ was used to filter DEGs from two groups
503 comparison (WT+LPS vs. WT+PBS, *Sh3*$^{+/-}$+LPS vs. *Sh3*$^{+/-}$+PBS, *Sh3*$^{+/}$+LPS vs.
504 WT+LPS and *Sh3*$^{+/-}$+PBS vs. WT+PBS) for genes comparison and analysis. *Pathway*
505 *analysis*: QIAGEN Ingenuity Pathway Analysis (IPA) library of canonical pathways was
506 used to identify the pathways most significant to the data set. Molecules from the dataset
507 meeting the criteria in which log_2fold cutoff threshold at 0.25 and $p < 0.05$ were associated
508 with a canonical pathway in the QIAGEN Knowledge Base were considered for the
509 analysis. Because using log_2fold cutoff threshold at 1 only revealed three activated
510 pathways in *Sh3*$^{+/}$+LPS vs. WT+LPS comparison which were all inflammation-related, so
511 we expanded the log_2fold cutoff threshold to 0.25. The significance of the association
512 between the data set and the canonical pathway was measured based on: 1) a ratio of
513 the number of molecules from the data set that map to the pathway divided by the total
514 number of molecules that map to the canonical pathway was displayed, 2) a right-tailed
515 Fisher's Exact Test was used to calculate a p-value determining the probability that the
516 association between the genes in the dataset and the canonical pathway was explained
517 by chance alone, 3) A z-score was calculated to indicate the likelihood of activation
518 or inhibition of that pathway. In this paper, pathways with right-tailed Fisher's Exact Test
519 $p < 0.05$, z-score > 0.1 was considered as activated pathways and z-score < -0.1 was
520 considered as inhibited pathways. The volcano plot was created using VolcaNoseR [92].
521 Veen diagram was plotted using InteractiVenn [93].

522 **Real-Time Quantitative Reverse Transcription PCR (RT-qPCR)**

523 Total RNA was isolated using same protocol as RNA-seq. RNA was transcribed
524 into cDNA using iScript cDNA Synthesis Kit (Bio-Rad, 1708890) and qPCR was performed
525 in triplicate using iQ SYBR Green Supermix (Bio-Rad, 1708880). Gene expressions were
526 normalized to the expression of GAPDH. Primers used to amplify cDNAs are: *Il1b,*
527 forward, TGGACCTTCCAGGATGAGGACA, reverse, GTTCATCTCGGAGCCTGTAGTG;
528 *Cxcl10,* forward, ATCATCCCTGCGAGCCTATCCT, reverse, GACCTTTTTTGGCTAAA
529 CGCTTTC; *Cx3cr1,* forward, GAGCATCACTGACATCTACCTCC, reverse, AGAAGGCA-
530 GTCGTGAGCTTGCA; *P2ry12* forward, CATTGACCGCTACCTGAAGACC, reverse,
531 GCCTCCTGTTGGTGAGAATCATG; *Gapdh* forward, CAAAATGGTGAAGGTCGGTG,
532 reverse, AATGAAGGGGTCGTTGATGG.

533 **Immunohistochemistry**

534 Transcardiac perfusion was conducted at both 3 hours and 24 hours after LPS or
535 PBS injection with 20 mL PBS then 20 mL 4% paraformaldehyde (PFA, Santa Cruz, sc-
536 281692). Mouse brains were collected, fixed in 4% PFA for 24 hours, then changed to 30%
537 (w/v) sucrose before sectioning. 50 μM brain sections between Bregma 1 mm to -1 mm
538 were obtained using vibratome (Leica, VT1200S) or using cryostat (Leica, CM1860).
539 Primary antibody including anti-rabbit-IBA1 (1:200, FUJIFILM Wako Chemicals, 019-
540 19741), anti-mouse-TLR4 (1:100, Abcam, ab22048), anti-rat-CD68 (1:100, Abcam,
541 ab53444), anti-mouse-vGluT1 (1:100, Synaptic Systems, 135511), anti-guineapig-
542 vGluT1 (1:200, Synaptic Systems, 135318) and anti-mouse-PSD95 (1:100, Invitrogen,
543 MA1-045), and secondary antibody including goat anti-mouse Alexa Fluor 488 (Abcam,
544 ab150113), donkey anti-mouse Alexa Fluor 488 (Abcam, ab150105), donkey anti-rabbit
545 Alexa Fluor 594 (Invitrogen, A-21207), goat anti-rat Alexa Fluor 594 (Invitrogen, A-11007),

546 goat anti-guineapig Alexa Fluor 647 (Abcam, ab150187), goat anti-rabbit Alexa Fluor 647
547 (Jackson ImmunoResearch, 111-605-144) were used at 1:500 dilution. Zeiss LSM 980
548 confocal microscopy with a 20X objective lens was used for wide-field IBA1 imaging, a
549 63X oil objective lens with Z stack (0.2 μm thickness/slice, total 30-40 slices/image) was
550 used for engulfment imaging, and Airyscan 2 with a 63X oil objective lens was used for
551 super-resolution imaging of vGluT1 and PSD95 colocalization. Zeiss LSM 900 confocal
552 microscopy with a 63X oil objective lens was used for TLR4/IBA1 co-staining imaging. In
553 total, 49 images at 3 hours and 52 images at 24 hours post-injection were analyzed for
554 IBA1 fluorescence intensity, 20 images were analyzed for IBA1/TLR4 colocalization, 47
555 images were analyzed for microglia engulfment, and 26 images at 24 hours and 61
556 images at 2 weeks post-injection were analyzed for vGluT1/PSD95 colocalization. Images
557 were randomly selected from cortex regions of brain slices. Immunostaining and imaging
558 were performed under same conditions and same settings at same time across different
559 groups within same cohort. Cohort 1 with 8 groups was for IBA1 staining. Cohort 2 with 2
560 groups for TLR4/IBA1 co-staining. Cohort 3 with 2 groups was for IBA1/CD68/vGluT1 co-
561 staining. Cohort 4 with 2 groups was for 24 hours post-injection vGluT1/PSD95 co-
562 staining. Cohort 5 with 4 groups was for 2 weeks post-injection vGluT1/PSD95 co-staining.
563 Biological triplicates of brain slices from one mouse brain were employed. Results from
564 at least three mouse brains per group were analyzed and compared. ImageJ software
565 was used for IBA1 fluorescence intensity quantification. Imaris software (Oxford
566 Instrument) was used for microglia engulfment 3D rendering analysis. ZEN Blue software
567 was used for colocalization analysis. See details on 3D rendering and colocalization
568 analysis protocols in the Supplementary Information.

569 **Western blot**

570 Western blot was performed as previously described [94]. Whole cell lysates from
571 mouse forebrain hemisphere were prepared using 1x lysis buffer (Cell Signaling
572 Technology, 9803S) containing 1x protease/phosphatase inhibitor (Cell Signaling
573 Technology, 5872S). Crude postsynaptic density (PSD) fraction from mouse forebrain
574 hemisphere were prepared following previously described protocol with some
575 modifications[35,95]. See details in Supplementary Information. Samples were boiled in 4x
576 Laemlli buffer (Bio-Rad, 161-0747) at 98 °C for 5 min before gel electrophoresis. Home-
577 made anti-rabbit SHANK3 C-terminus monoclonal antibody (1:1000), anti-rabbit TLR4
578 monoclonal antibody (1:1000, Santa Cruz, sc-293072), anti-mouse PSD95 monoclonal
579 antibody (1:1000, Invitrogen, MA1-046), HOMER 1b/c monoclonal HRP-conjugated
580 antibody (1:1000, Santa Cruz, sc-17842-HRP), anti-rabbit GluA1 (AMPA receptor)
581 polyclonal antibody (1:1000, Abcam, ab31232), anti-NR2A (NMDA receptor) polyclonal
582 antibody (1:1000, Millipore, ab31232), and β-ACTIN monoclonal HRP-conjugated
583 antibody (1:1000, Invitrogen, MA5-15739-HRP) were used.

584 **Statistical analysis**

585 Graphpad Prism 10.0 (GraphPad Software) was used for the statistical analysis
586 and data plot. Differences were analyzed by student's *t*-test if comparing two variables or
587 using ANOVA if comparing more than two variables followed by multiple comparisons
588 either using statistical hypothesis testing with correction or planned comparisons without
589 correction. Significance was determined by two-tailed *t*-test *p* value or multiplicity adjusted
590 *p* value. For data, which was not sampled from Gaussian distribution, a nonparametric
591 test was performed. Since unequal variance observed in LPS-evoked cytokines and

592 chemokines, Brown-Forsythe and Welch ANOVA tests were performed (**Fig. 4A-B**). See
593 detailed statistical analysis for each figure in **Supplementary Table 5**. n represents the
594 total number of data points per group, usually meaning the mice number with an exception
595 that n represents number of images in immunohistochemistry results. Both sexes of mice
596 were used and balanced across genotype and treatment, with an exception that WT+PBS
597 and WT+LPS groups were all male mice in RNA-seq experiments. Behavioral difference
598 between male and female mice were explored in **Supplementary Fig. 1**. In box plot,
599 individual data points were plotted as: whiskers go down to the smallest value and up to
600 the largest value, box extends from the 25th to 75th percentiles and line in the middle of
601 the box is plotted at the median. In bar graph, individual data points were plotted and
602 presented as average ± SEM. $p < 0.05$ was considered statistically significant. BioRender
603 was used to create schematic diagram.

604 **Authorship contribution statement**

605 S-N.Q. and Y-H.J. designed the experiments. S-N.Q. collected and analyzed the data.
606 S.W. manually scored grooming behavior. S.W., K-Y.K. and S.J. performed western blot.
607 S-N.Q. and Y-H.J. wrote and revised the manuscripts.

608 **Acknowledgement**

609 This work was supported by the National Institutes of Health (NIH) grant HD088007
610 MH104316, MH098114, MH117289, HD087795 (Y-H.J), the Autism Science Foundation
611 (ASF) fellowship (S-N.Q), and the National Research Foundation of Korea (NRF) grant
612 (RS-2024-00401971 (S.J), Brain Pool program RS-2024-00409006 (S.E.W)). This work
613 was supported by the rodent behavior analysis facility and imaging core facility in Yale
614 University funded by the Kavli Institute of Neuroscience. The bulk RNA sequencing was
615 supported by the National Institute of General Medical Sciences of the National Institutes
616 of Health under Award Number 1S10OD030363-01A1.

617 **Conflict of Interest**

618 There are no competing financial interests in relation to the work described.

619 **Reference**

620 1 Regier, D. A., Kuhl, E. A. & Kupfer, D. J. The DSM-5: Classification and criteria changes.
621 *World Psychiatry* **12**, 92-98 (2013). https://doi.org/10.1002/wps.20050

622 2 Stefanatos, G. A. Regression in autistic spectrum disorders. *Neuropsychol Rev* **18**,
623 305-319 (2008). https://doi.org/10.1007/s11065-008-9073-y

624 3 Manelis, L. *et al.* Language regression is associated with faster early motor
625 development in children with autism spectrum disorder. *Autism Res* **13**, 145-156
626 (2020). https://doi.org/10.1002/aur.2197

627 4 Boterberg, S., Van Coster, R. & Roeyers, H. Characteristics, Early Development and
628 Outcome of Parent-Reported Regression in Autism Spectrum Disorder. *J Autism Dev*
629 *Disord* **49**, 4603-4625 (2019). https://doi.org/10.1007/s10803-019-04183-x

630 5 Kohlenberg, T. M. *et al.* Psychiatric illness and regression in individuals with Phelan-
631 McDermid syndrome. *J Neurodev Disord* **12**, 7 (2020).
632 https://doi.org/10.1186/s11689-020-9309-6

633 6 Ghaziuddin, M. Catatonia: A Common Cause of Late Regression in Autism. *Front*
634 *Psychiatry* **12**, 674009 (2021). https://doi.org/10.3389/fpsyt.2021.674009

635 7 Betancur, C. & Buxbaum, J. D. SHANK3 haploinsufficiency: a "common" but
636 underdiagnosed highly penetrant monogenic cause of autism spectrum disorders.
637 *Mol Autism* **4**, 17 (2013). https://doi.org/10.1186/2040-2392-4-17

638 8 Satterstrom, F. K. *et al.* Large-Scale Exome Sequencing Study Implicates Both
639 Developmental and Functional Changes in the Neurobiology of Autism. *Cell* **180**,
640 568-584 e523 (2020). https://doi.org/10.1016/j.cell.2019.12.036

641 9 Zhou, X. *et al*. Integrating de novo and inherited variants in 42,607 autism cases
642 identifies mutations in new moderate-risk genes. *Nat Genet* (2022).
643 https://doi.org/10.1038/s41588-022-01148-2
644 10 Fu, J. M. *et al*. Rare coding variation provides insight into the genetic architecture and
645 phenotypic context of autism. *Nat Genet* (2022). https://doi.org/10.1038/s41588-
646 022-01104-0
647 11 Nevado, J. *et al*. Variability in Phelan-McDermid Syndrome in a Cohort of 210
648 Individuals. *Front Genet* **13**, 652454 (2022).
649 https://doi.org/10.3389/fgene.2022.652454
650 12 Soorya, L. *et al*. Prospective investigation of autism and genotype-phenotype
651 correlations in 22q13 deletion syndrome and SHANK3 deficiency. *Mol Autism* **4**, 18
652 (2013). https://doi.org/10.1186/2040-2392-4-18
653 13 Leblond, C. S. *et al*. Meta-analysis of SHANK Mutations in Autism Spectrum Disorders:
654 a gradient of severity in cognitive impairments. *PLoS Genet* **10**, e1004580 (2014).
655 https://doi.org/10.1371/journal.pgen.1004580
656 14 Serrada-Tejeda, S., Martínez-Piédrola, R. M., Máximo-Bocanegra, N., Sánchez-
657 Herrera-Baeza, P. & Pérez-de-Heredia-Torres, M. Descriptive Analysis of Adaptive
658 Behavior in Phelan-McDermid Syndrome and Autism Spectrum Disorder. *Frontiers in*
659 *neuroscience* **16**, 893003 (2022). https://doi.org/10.3389/fnins.2022.893003
660 15 Reierson, G. *et al*. Characterizing regression in Phelan McDermid Syndrome (22q13
661 deletion syndrome). *J Psychiatr Res* **91**, 139-144 (2017).
662 https://doi.org/10.1016/j.jpsychires.2017.03.010

663 16 Denayer, A. *et al*. Neuropsychopathology in 7 Patients with the 22q13 Deletion
664 Syndrome: Presence of Bipolar Disorder and Progressive Loss of Skills. *Molecular*
665 *Syndromology* **3**, 14-20 (2012). https://doi.org/10.1159/000339119
666 17 Zwanenburg, R. J., Ruiter, S. A. J., van den Heuvel, E. R., Flapper, B. C. T. & Van
667 Ravenswaaij-Arts, C. M. A. Developmental phenotype in Phelan-McDermid (22q13.3
668 deletion) syndrome: a systematic and prospective study in 34 children. *Journal of*
669 *Neurodevelopmental Disorders* **8**, 16 (2016). https://doi.org/10.1186/s11689-016-
670 9150-0
671 18 Serret, S. *et al*. Lithium as a rescue therapy for regression and catatonia features in
672 two SHANK3 patients with autism spectrum disorder: case reports. *BMC Psychiatry*
673 **15**, 107 (2015). https://doi.org/10.1186/s12888-015-0490-1
674 19 Phelan, K. & McDermid, H. E. The 22q13.3 Deletion Syndrome (Phelan-McDermid
675 Syndrome). *Mol Syndromol* **2**, 186-201 (2012). https://doi.org/10.1159/000334260
676 20 Phelan, K. *et al*. Phelan-McDermid syndrome: a classification system after 30 years
677 of experience. *Orphanet J Rare Dis* **17**, 27 (2022). https://doi.org/10.1186/s13023-
678 022-02180-5
679 21 Bey, A. L. *et al*. Subacute Neuropsychiatric Syndrome in Girls With SHANK3 Mutations
680 Responds to Immunomodulation. *Pediatrics* **145**, e20191490 (2020).
681 https://doi.org/10.1542/peds.2019-1490
682 22 Durand, C. M. *et al*. Mutations in the gene encoding the synaptic scaffolding protein
683 SHANK3 are associated with autism spectrum disorders. *Nat Genet* **39**, 25-27 (2007).
684 https://doi.org/10.1038/ng1933

685 23 He, G. *et al.* Dexmedetomidine attenuates neuroinflammation and microglia
686 activation in LPS-stimulated BV2 microglia cells through targeting circ-Shank3/miR-
687 140-3p/TLR4 axis. *Eur J Histochem* **67** (2023). https://doi.org/10.4081/ejh.2023.3766
688 24 Fischer, I. *et al.* Hyperbaric Oxygen Therapy Alleviates Social Behavior Dysfunction
689 and Neuroinflammation in a Mouse Model for Autism Spectrum Disorders. *Int J Mol*
690 *Sci* **23** (2022). https://doi.org/10.3390/ijms231911077
691 25 Cope, E. C. *et al.* Immature Neurons and Radial Glia, But Not Astrocytes or Microglia,
692 Are Altered in Adult Cntnap2 and Shank3 Mice, Models of Autism. *eNeuro* **3** (2016).
693 https://doi.org/10.1523/eneuro.0196-16.2016
694 26 Urrutia-Ruiz, C. *et al.* Deletion of the Autism-Associated Protein SHANK3 Abolishes
695 Structural Synaptic Plasticity after Brain Trauma. *Int J Mol Sci* **23** (2022).
696 https://doi.org/10.3390/ijms23116081
697 27 Eyo, U. & Molofsky, A. V. Defining microglial-synapse interactions. *Science* **381**, 1155-
698 1156 (2023). https://doi.org/doi:10.1126/science.adh7906
699 28 Pereira-Iglesias, M. *et al.* Microglia as hunters or gatherers of brain synapses. *Nature*
700 *Neuroscience* **28**, 15-23 (2025). https://doi.org/10.1038/s41593-024-01818-w
701 29 Suzuki, K. *et al.* Microglial activation in young adults with autism spectrum disorder.
702 *JAMA Psychiatry* **70**, 49-58 (2013). https://doi.org/10.1001/jamapsychiatry.2013.272
703 30 Kumar, A., Williams, M. T. & Chugani, H. T. Evaluation of basal ganglia and thalamic
704 inflammation in children with pediatric autoimmune neuropsychiatric disorders
705 associated with streptococcal infection and tourette syndrome: a positron emission

706 tomographic (PET) study using 11C-[R]-PK11195. *J Child Neurol* **30**, 749-756 (2015).
707 https://doi.org/10.1177/0883073814543303
708 31 Han, V. X., Patel, S., Jones, H. F. & Dale, R. C. Maternal immune activation and
709 neuroinflammation in human neurodevelopmental disorders. *Nature Reviews*
710 *Neurology* **17**, 564-579 (2021). https://doi.org/10.1038/s41582-021-00530-8
711 32 Michels, S., Mali, A., Jäntti, H., Rezaie, M. & Malm, T. Microglial involvement in autism
712 spectrum disorder: insights from human data and iPSC models. *Brain, Behavior, and*
713 *Immunity* **130**, 106071 (2025).
714 https://doi.org/https://doi.org/10.1016/j.bbi.2025.106071
715 33 Tzanoulinou, S. *et al*. Inhibition of Trpv4 rescues circuit and social deficits unmasked
716 by acute inflammatory response in a Shank3 mouse model of Autism. *Molecular*
717 *Psychiatry* **27**, 2080-2094 (2022). https://doi.org/10.1038/s41380-021-01427-0
718 34 Zhang, L. *et al*. SHANK3 in vagal sensory neurons regulates body temperature,
719 systemic inflammation, and sepsis. *Front Immunol* **14**, 1124356 (2023).
720 https://doi.org/10.3389/fimmu.2023.1124356
721 35 Wang, X. *et al*. Altered mGluR5-Homer scaffolds and corticostriatal connectivity in a
722 Shank3 complete knockout model of autism. *Nat Commun* **7**, 11459 (2016).
723 https://doi.org/10.1038/ncomms11459
724 36 Piirsalu, M. *et al*. Treatment With Lipopolysaccharide Induces Distinct Changes in
725 Metabolite Profile and Body Weight in 129Sv and Bl6 Mouse Strains. *Frontiers in*
726 *Pharmacology* **11** (2020). https://doi.org/10.3389/fphar.2020.00371

727 37 Jung, H. *et al*. LPS induces microglial activation and GABAergic synaptic deficits in
728 the hippocampus accompanied by prolonged cognitive impairment. *Scientific*
729 *Reports* **13**, 6547 (2023). https://doi.org/10.1038/s41598-023-32798-9
730 38 Decker Ramirez, E. B. *et al*. The effects of lipopolysaccharide exposure on social
731 interaction, cytokine expression, and alcohol consumption in male and female mice.
732 *Physiology & Behavior* **265**, 114159 (2023).
733 https://doi.org/https://doi.org/10.1016/j.physbeh.2023.114159
734 39 O'Connor, J. C. *et al*. Lipopolysaccharide-induced depressive-like behavior is
735 mediated by indoleamine 2,3-dioxygenase activation in mice. *Mol Psychiatry* **14**, 511-
736 522 (2009). https://doi.org/10.1038/sj.mp.4002148
737 40 Parrott, J. M., Oster, T. & Lee, H. Y. Altered inflammatory response in FMRP-deficient
738 microglia. *iScience* **24**, 103293 (2021). https://doi.org/10.1016/j.isci.2021.103293
739 41 Hodges, S. L. *et al*. Lipopolysaccharide-induced inflammation leads to acute
740 elevations in pro-inflammatory cytokine expression in a mouse model of Fragile X
741 syndrome. *Physiol Behav* **215**, 112776 (2020).
742 https://doi.org/10.1016/j.physbeh.2019.112776
743 42 Eliopoulos, A. G., Dumitru, C. D., Wang, C. C., Cho, J. & Tsichlis, P. N. Induction of
744 COX-2 by LPS in macrophages is regulated by Tpl2-dependent CREB activation
745 signals. *Embo j* **21**, 4831-4840 (2002). https://doi.org/10.1093/emboj/cdf478
746 43 Blais, V., Turrin, N. P. & Rivest, S. Cyclooxygenase 2 (COX-2) inhibition increases the
747 inflammatory response in the brain during systemic immune stimuli. *J Neurochem* **95**,
748 1563-1574 (2005). https://doi.org/10.1111/j.1471-4159.2005.03480.x

749 44 Cimolai, N. The potential and promise of mefenamic acid. *Expert Review of Clinical*
750 *Pharmacology* **6**, 289-305 (2013). https://doi.org/10.1586/ecp.13.15
751 45 Khansari, P. S. & Halliwell, R. F. Evidence for neuroprotection by the fenamate NSAID,
752 mefenamic acid. *Neurochemistry International* **55**, 683-688 (2009).
753 https://doi.org/https://doi.org/10.1016/j.neuint.2009.06.014
754 46 Lu, X. *et al*. Transcriptional determinism and stochasticity contribute to the
755 complexity of autism-associated SHANK family genes. *Cell Rep* **43**, 114376 (2024).
756 https://doi.org/10.1016/j.celrep.2024.114376
757 47 Krämer, A., Green, J., Pollard, J., Jr. & Tugendreich, S. Causal analysis approaches in
758 Ingenuity Pathway Analysis. *Bioinformatics* **30**, 523-530 (2014).
759 https://doi.org/10.1093/bioinformatics/btt703
760 48 Sousa, C. *et al*. Single-cell transcriptomics reveals distinct inflammation-induced
761 microglia signatures. *EMBO Rep* **19** (2018).
762 https://doi.org/10.15252/embr.201846171
763 49 Norden, D. M., Trojanowski, P. J., Villanueva, E., Navarro, E. & Godbout, J. P.
764 Sequential activation of microglia and astrocyte cytokine expression precedes
765 increased Iba-1 or GFAP immunoreactivity following systemic immune challenge.
766 *Glia* **64**, 300-316 (2016). https://doi.org/10.1002/glia.22930
767 50 Tiwari, P. C. & Pal, R. The potential role of neuroinflammation and transcription
768 factors in Parkinson disease. *Dialogues Clin Neurosci* **19**, 71-80 (2017).
769 https://doi.org/10.31887/DCNS.2017.19.1/rpal

770 51 Cartarozzi, L. P., de Melo Lima, B. H., Tomiyama, A. L. R. M., Santos, F. R. & de Oliveira,
771 A. L. R. Toll-like receptors 2 and 4 influence neuronal survival and glial reactions
772 following ventral root crush injury in mice. *Journal of Neuroimmunology* **406**, 578655
773 (2025). https://doi.org/https://doi.org/10.1016/j.jneuroim.2025.578655
774 52 Yao, L. *et al*. Toll-like receptor 4 mediates microglial activation and production of
775 inflammatory mediators in neonatal rat brain following hypoxia: role of TLR4 in
776 hypoxic microglia. *Journal of Neuroinflammation* **10**, 785 (2013).
777 https://doi.org/10.1186/1742-2094-10-23
778 53 Jiang, Y. *et al*. Evobrutinib mitigates neuroinflammation after ischemic stroke by
779 targeting M1 microglial polarization via the TLR4/Myd88/NF-κB pathway. *Mol Med* **31**,
780 148 (2025). https://doi.org/10.1186/s10020-025-01203-8
781 54 Zhu, J. *et al*. Toll-like receptor 4 deficiency in Purkinje neurons drives cerebellar ataxia
782 by impairing the BK channel-mediated after-hyperpolarization and cytosolic calcium
783 homeostasis. *Cell Death Dis* **15**, 594 (2024). https://doi.org/10.1038/s41419-024-
784 06988-w
785 55 *TLR4 expression in the Human Protein Atlas*,
786 <https://www.proteinatlas.org/ENSG00000136869-TLR4/single+cell> (
787 56 Sjöstedt, E. *et al*. An atlas of the protein-coding genes in the human, pig, and mouse
788 brain. *Science* **367**, eaay5947 (2020). https://doi.org/10.1126/science.aay5947
789 57 Chen, X. *et al*. PSD-95 family MAGUKs are essential for anchoring AMPA and NMDA
790 receptor complexes at the postsynaptic density. *Proc Natl Acad Sci U S A* **112**, E6983-
791 6992 (2015). https://doi.org/10.1073/pnas.1517045112

792 58 Jaiswal, H. *et al*. The NF-κB regulator Bcl-3 restricts terminal differentiation and
793 promotes memory cell formation of CD8+ T cells during viral infection. *PLoS Pathog*
794 **17**, e1009249 (2021). https://doi.org/10.1371/journal.ppat.1009249
795 59 Pelisch, N., Rosas Almanza, J., Stehlik, K. E., Aperi, B. V. & Kroner, A. CCL3 contributes
796 to secondary damage after spinal cord injury. *J Neuroinflammation* **17**, 362 (2020).
797 https://doi.org/10.1186/s12974-020-02037-3
798 60 Klein, R. S. Regulation of neuroinflammation: the role of CXCL10 in lymphocyte
799 infiltration during autoimmune encephalomyelitis. *J Cell Biochem* **92**, 213-222 (2004).
800 https://doi.org/10.1002/jcb.20052
801 61 Zhong, K. *et al*. A Synthetic Steroid 5α-Androst-3β, 5, 6β-triol Alleviates Radiation-
802 Induced Brain Injury in Mice via Inhibiting GBP5/NF-κB/NLRP3 Signal Axis. *Mol*
803 *Neurobiol* **61**, 4074-4089 (2024). https://doi.org/10.1007/s12035-023-03831-9
804 62 Han, J. H. *et al*. IFITM6 expression is increased in macrophages of tumor-bearing mice.
805 *Oncol Rep* **25**, 531-536 (2011). https://doi.org/10.3892/or.2010.1092
806 63 Cunningham, C., Wilcockson, D. C., Campion, S., Lunnon, K. & Perry, V. H. Central
807 and systemic endotoxin challenges exacerbate the local inflammatory response and
808 increase neuronal death during chronic neurodegeneration. *J Neurosci* **25**, 9275-
809 9284 (2005). https://doi.org/10.1523/jneurosci.2614-05.2005
810 64 Zhao, J. *et al*. STEAP4 expression in CNS resident cells promotes Th17 cell-induced
811 autoimmune encephalomyelitis. *J Neuroinflammation* **18**, 98 (2021).
812 https://doi.org/10.1186/s12974-021-02146-7

813 65 Lester, S. N. & Li, K. Toll-like receptors in antiviral innate immunity. *J Mol Biol* **426**,
814 1246-1264 (2014). https://doi.org/10.1016/j.jmb.2013.11.024
815 66 Li, Y. *et al*. The multifaceted roles of activating transcription factor 3 (ATF3) in
816 inflammatory responses - Potential target to regulate neuroinflammation in acute
817 brain injury. *J Cereb Blood Flow Metab* **43**, 8-17 (2023).
818 https://doi.org/10.1177/0271678x231171999
819 67 Ross, J. L. *et al*. Microglia and monocyte-derived macrophages drive progression of
820 pediatric high-grade gliomas and are transcriptionally shaped by histone mutations.
821 *Immunity* **57**, 2669-2687.e2666 (2024).
822 https://doi.org/10.1016/j.immuni.2024.09.007
823 68 Krzyzowska, M., Kowalczyk, A., Skulska, K., Thörn, K. & Eriksson, K. Fas/FasL
824 Contributes to HSV-1 Brain Infection and Neuroinflammation. *Front Immunol* **12**,
825 714821 (2021). https://doi.org/10.3389/fimmu.2021.714821
826 69 Wu, S. *et al*. HSPA1A Protects Cells from Thermal Stress by Impeding ESCRT-0–
827 Mediated Autophagic Flux in Epidermal Thermoresistance. *Journal of Investigative*
828 *Dermatology* **141**, 48-58.e43 (2021).
829 https://doi.org/https://doi.org/10.1016/j.jid.2020.05.105
830 70 Kampinga, H. H. *et al*. Guidelines for the nomenclature of the human heat shock
831 proteins. *Cell Stress and Chaperones* **14**, 105-111 (2009).
832 https://doi.org/https://doi.org/10.1007/s12192-008-0068-7

833 71 Frankiw, L., Mann, M., Li, G., Joglekar, A. & Baltimore, D. Alternative splicing coupled
834 with transcript degradation modulates OAS1g antiviral activity. *Rna* **26**, 126-136
835 (2020). https://doi.org/10.1261/rna.073825.119
836 72 Bao, Z. *et al*. Prokineticin-2 prevents neuronal cell deaths in a model of traumatic
837 brain injury. *Nat Commun* **12**, 4220 (2021). https://doi.org/10.1038/s41467-021-
838 24469-y
839 73 Lei, J., Deng, Y. & Ma, S. Downregulation of TGIF2 is possibly correlated with neuronal
840 apoptosis and autism-like symptoms in mice. *Brain Behav* **12**, e2610 (2022).
841 https://doi.org/10.1002/brb3.2610
842 74 Dhossche, D. *et al*. Early-onset catatonia associated with SHANK3 mutations:
843 looking at the autism spectrum through the prism of psychomotor phenomena. *Front*
844 *Psychiatry* **14**, 1186555 (2023). https://doi.org/10.3389/fpsyt.2023.1186555
845 75 Srivastava, S. *et al*. Updated consensus guidelines on the management of Phelan-
846 McDermid syndrome. *Am J Med Genet A* **191**, 2015-2044 (2023).
847 https://doi.org/10.1002/ajmg.a.63312
848 76 Yurumez, E., Temelturk, R. D., Kaymak, B., Karabıyıkoğlu, Y. & Zengin, N. D. Catatonia
849 in autism spectrum disorders: Prevalence, functional impact, and diagnostic insights.
850 *Psychiatry Res* **342**, 116250 (2024). https://doi.org/10.1016/j.psychres.2024.116250
851 77 Monville, C., Torres, E. M. & Dunnett, S. B. Comparison of incremental and
852 accelerating protocols of the rotarod test for the assessment of motor deficits in the
853 6-OHDA model. *J Neurosci Methods* **158**, 219-223 (2006).
854 https://doi.org/10.1016/j.jneumeth.2006.06.001

855 78 Hernandez, A. R., Truckenbrod, L. M., Campos, K. T., Williams, S. A. & Burke, S. N. Sex
856 differences in age-related impairments vary across cognitive and physical
857 assessments in rats. *Behav Neurosci* **134**, 69-81 (2020).
858 https://doi.org/10.1037/bne0000352
859 79 Han, J., Fan, Y., Zhou, K., Blomgren, K. & Harris, R. A. Uncovering sex differences of
860 rodent microglia. *Journal of Neuroinflammation* **18**, 74 (2021).
861 https://doi.org/10.1186/s12974-021-02124-z
862 80 Hines, D. J., Choi, H. B., Hines, R. M., Phillips, A. G. & MacVicar, B. A. Prevention of
863 LPS-induced microglia activation, cytokine production and sickness behavior with
864 TLR4 receptor interfering peptides. *PLoS One* **8**, e60388 (2013).
865 https://doi.org/10.1371/journal.pone.0060388
866 81 Han, Q. *et al*. SHANK3 Deficiency Impairs Heat Hyperalgesia and TRPV1 Signaling in
867 Primary Sensory Neurons. *Neuron* **92**, 1279-1293 (2016).
868 https://doi.org/10.1016/j.neuron.2016.11.007
869 82 Kim, Y. E. *et al*. Endothelial SHANK3 regulates tight junctions in the neonatal mouse
870 blood-brain barrier through β-Catenin signaling. *Nat Commun* **16**, 1407 (2025).
871 https://doi.org/10.1038/s41467-025-56720-1
872 83 Atanasova, E. *et al*. Immune activation during pregnancy exacerbates ASD-related
873 alterations in Shank3-deficient mice. *Mol Autism* **14**, 1 (2023).
874 https://doi.org/10.1186/s13229-022-00532-3

875 84 Leblond, C. S. *et al*. Meta-analysis of SHANK Mutations in Autism Spectrum Disorders:
876 A Gradient of Severity in Cognitive Impairments. *PLOS Genetics* **10**, e1004580 (2014).
877 https://doi.org/10.1371/journal.pgen.1004580
878 85 Jesse, S. *et al*. Phelan McDermid Syndrome: Multiple Sclerosis as a Rare but Treatable
879 Cause for Regression-A Case Report. *Int J Mol Sci* **22** (2021).
880 https://doi.org/10.3390/ijms22052311
881 86 Faul, F., Erdfelder, E., Lang, A. G. & Buchner, A. G*Power 3: a flexible statistical power
882 analysis program for the social, behavioral, and biomedical sciences. *Behav Res*
883 *Methods* **39**, 175-191 (2007). https://doi.org/10.3758/bf03193146
884 87 Bourin, M. & Hascoët, M. The mouse light/dark box test. *European Journal of*
885 *Pharmacology* **463**, 55-65 (2003). https://doi.org/https://doi.org/10.1016/S0014-
886 2999(03)01274-3
887 88 Moy, S. S. *et al*. Mouse behavioral tasks relevant to autism: phenotypes of 10 inbred
888 strains. *Behav Brain Res* **176**, 4-20 (2007). https://doi.org/10.1016/j.bbr.2006.07.030
889 89 Kim, D., Paggi, J. M., Park, C., Bennett, C. & Salzberg, S. L. Graph-based genome
890 alignment and genotyping with HISAT2 and HISAT-genotype. *Nature Biotechnology* **37**,
891 907-915 (2019). https://doi.org/10.1038/s41587-019-0201-4
892 90 Pertea, M. *et al*. StringTie enables improved reconstruction of a transcriptome from
893 RNA-seq reads. *Nature Biotechnology* **33**, 290-295 (2015).
894 https://doi.org/10.1038/nbt.3122

895 91 Love, M. I., Huber, W. & Anders, S. Moderated estimation of fold change and
896 dispersion for RNA-seq data with DESeq2. *Genome Biol* **15**, 550 (2014).
897 https://doi.org/10.1186/s13059-014-0550-8
898 92 Goedhart, J. & Luijsterburg, M. S. VolcaNoseR is a web app for creating, exploring,
899 labeling and sharing volcano plots. *Scientific Reports* **10**, 20560 (2020).
900 https://doi.org/10.1038/s41598-020-76603-3
901 93 Heberle, H., Meirelles, G. V., da Silva, F. R., Telles, G. P. & Minghim, R. InteractiVenn: a
902 web-based tool for the analysis of sets through Venn diagrams. *BMC Bioinformatics*
903 **16**, 169 (2015). https://doi.org/10.1186/s12859-015-0611-3
904 94 Wang, S. E. *et al*. TRPV1 Regulates Stress Responses through HDAC2. *Cell Rep* **19**,
905 401-412 (2017). https://doi.org/10.1016/j.celrep.2017.03.050
906 95 Carlin, R. K., Grab, D. J., Cohen, R. S. & Siekevitz, P. Isolation and characterization of
907 postsynaptic densities from various brain regions: enrichment of different types of
908 postsynaptic densities. *J Cell Biol* **86**, 831-845 (1980).
909 https://doi.org/10.1083/jcb.86.3.831

910

911 **Figure legend:**

912 **Figure 1. LPS challenge induced selective behavioral impairments in *Sh3*$^{+/-}$ mice.**

913 **A. The body weight loss after LPS intraperitoneal injection.** Mouse was weighed
914 before injection, and at 3, 6, 24, 48, and 72 hours after LPS (1 mg/kg) or the same volume
915 of PBS injection. Each mouse's body weight was normalized to the weight before injection.
916 Two-way repeated measures ANOVA was performed (genotype/LPS effect $F_{(3, 50)} = 34.32$,
917 $p < 0.0001$; Hour effect $F_{(4, 200)} = 84.15$, $p < 0.0001$; genotype/LPS X Hour interaction F
918 $_{(12, 200)} = 22.64$, $p < 0.0001$). Post-hoc Tuckey's test showed no significant difference
919 between WT+PBS (n = 8) and *Sh3*$^{+/-}$+PBS (n = 17) or between WT+LPS (n = 8) and
920 *Sh3*$^{+/-}$+LPS (n = 21) at 3 hours, 6 hours, 24 hours, 48 hours and 72 hours after injection.
921 Mouse body weight started to reduce significantly after LPS injection compared to PBS
922 injection at 24 hours, 48 hours and 72 hours. Mouse body weight from LPS groups
923 significantly increased at 72 hours compared to 48 hours after injection in both WT+LPS
924 and *Sh3*$^{+/-}$+LPS groups. See multiple comparison statistics in Supplementary Table 5.

925 **B. Schematic drawing for the experimental design.**

926 **C-D. LPS challenge impaired motor function in *Sh3*$^{+/-}$ mice.** Steady speed rotarod (16
927 rpm, **C**) and accelerated speed rotarod (4-40 rpm, **D**) tests were performed and latency
928 to fall was measured. No significant difference was found between WT+PBS and *Sh3*$^{+/-}$
929 +PBS (16 rpm, p =0.5487, 4-40 rpm, p =0.3283) or between WT+PBS and WT+LPS (16
930 rpm, p =0.9797, 4-40 rpm, p =0.6711). *Sh3*$^{+/-}$+LPS significantly reduced latency to fall
931 compared to *Sh3*$^{+/-}$+PBS (16 rpm, p =0.0126, 4-40 rpm, p =0.0061) or compared to

932 WT+LPS (16 rpm, p =0.002, 4-40 rpm, p =0.001). *Sh3*$^{-/-}$ mice significantly reduced latency
933 to fall compared to WT+PBS (16 rpm, $p < 0.0001$, 4-40 rpm, $p < 0.0001$).

934 **E-F. LPS challenge increased anxiety-like behavior in *Sh3*$^{+/-}$ mice.** Mouse duration
935 spent in the center of the open field test and travel distance in light chamber of light/dark
936 box test were measured. No significant difference found between WT+PBS and WT+LPS
937 (OFT, p = 0.5956, light/dark box p = 0.6004). *Sh3*$^{+/-}$+LPS showed less center duration
938 than *Sh3*$^{+/-}$+PBS (p = 0.0033) despite that *Sh3*$^{+/-}$+PBS showed increased center duration
939 than WT+PBS (p = 0.0005), and *Sh3*$^{+/-}$+LPS showed less travel distance in light chamber
940 than *Sh3*$^{+/-}$+PBS (p = 0.0158) or WT+LPS (p = 0.0107).

941 **G. LPS challenge increased repetitive behavior in *Sh3*$^{+/-}$ mice.** Grooming behavior
942 was hand scored and compared. *Sh3*$^{+/-}$+LPS showed longer grooming duration than
943 *Sh3*$^{+/-}$+PBS (p = 0.0348) or WT+LPS (p = 0.0135).

944 **H-I. LPS challenge had no effect on sociability *Sh3*$^{+/-}$ mice.** Three-chamber tests were
945 conducted and duration spent in mouse chamber (S), empty chamber (E), proximity
946 regions in mouse chamber (SP) and empty chamber (EP) were compared (Two-way
947 repeated measures ANOVA. **H.** genotype effect $F_{(4, 68)} = 1.590$, p = 0.1869, S/E effect F
948 $_{(1, 68)} = 25.46$, $p < 0.0001$, genotype X S/E interaction $F_{(4, 68)} = 0.8135$, p = 0.5209; **I.**
949 genotype effect $F_{(4, 68)} = 1.398$, p = 0.2441, SP/EP effect $F_{(1, 68)} = 34$, $p < 0.0001$, genotype
950 X SP/EP interaction $F_{(4, 68)} = 0.4236$, p = 0.7911). No significant difference of duration
951 was found between S vs. E (p = 0.5325) or SP vs. EP (p = 0.2529) in *Sh3*$^{-/-}$ mice. All other
952 groups of mice showed significantly increased duration in S vs. E or SP vs. EP. * $p < 0.05$,
953 ** $p < 0.005$, *** $p < 0.0005$, **** $p < 0.0001$

954 **Figure 2. Mefenamic acid (MFA) partially improved the motor behavior deterioration**
955 **in WT and *Sh3*$^{+/-}$ mice.**

956 **A. Schematic drawing for experiment design.** Anti-inflammatory treatment with
957 intraperitoneal MFA injection was given to mice once every day for 7 days after LPS
958 injection. Rotarod tests were performed 24 hours after the last does of MFA injection.

959 **B-C. MFA partially improved the rotarod test performance.** After 1-week treatment of
960 MFA, Steady speed rotarod (16 rpm, **B**) and accelerated speed rotarod (4-40 rpm, **C**)
961 tests were performed and latency to fall was compared. (Two-way ANOVA, **B. 16 rpm,**
962 LPS/MFA effect $F_{(1, 37)} = 23.66$, $p < 0.0001$, genotype effect $F_{(1,46)} = 1.859$, $p = 0.1794$,
963 LPS/MFA X genotype interaction $F_{(1, 37)} = 0.8697$, $p = 0.3571$. **C. 4-40 rpm,** LPS/MFA
964 effect $F_{(1, 85)} = 1.721$, $p = 0.1932$, genotype effect $F_{(1,85)} = 4.822$, $p = 0.0308$, LPS/MFA X
965 genotype interaction $F_{(1, 85)} = 0.8220$, $p = 0.3672$). Compared to vehicle group, MFA-
966 treated *Sh3*$^{+/-}$ and WT mice showed increased latency to fall in 16 rpm rotarod test (*Sh3*$^{+/-}$,
967 $p = 0.0091$; WT, $p = 0.0002$).

968 **D-E. MFA treatment was more effective in female *Sh3*$^{+/-}$ mice than male ones.** Two-
969 way ANOVA was performed to compare sex difference in MFA treatment (**D. 16 rpm,**
970 LPS/MFA effect $F_{(1, 43)} = 4.626$, $p = 0.0372$, sex effect $F_{(1,43)} = 9.227$, $p = 0.004$, LPS/MFA
971 X sex interaction $F_{(1, 43)} = 1.858$, $p = 0.1799$. **E. 4-40 rpm,** LPS/MFA effect $F_{(1, 16)} = 2.065$,
972 $p = 0.17$, sex effect $F_{(1,29)} = 2.369$, $p = 0.1346$, LPS/MFA X sex interaction $F_{(1, 16)} = 8.046$,
973 $p = 0.0119$). MFA-treated female *Sh3*$^{+/-}$ showed significantly higher latency to fall
974 compared to vehicle-treated female *Sh3*$^{+/-}$ (16 rpm, $p = 0.0229$; 40rpm, $p = 0.0106$) and
975 MFA-treated male *Sh3*$^{+/-}$ (16 rpm, $p = 0.0009$; 40rpm, $p = 0.0011$). * $p < 0.05$, ** $p < 0.005$,
976 *** $p < 0.0005$, **** $p < 0.0001$

977 **Figure 3. Bulk RNA sequencing revealed distinct molecular mechanism underlying**
978 **LPS effect on *Sh3*$^{+/-}$ mice.**

979 **A-D. The volcano plot shows differentially expressed genes (DEGs) distribution.**
980 DEGs were identified in four comparisons: *Sh3*$^{+/-}$+LPS vs *Sh3*$^{+/-}$+PBS (**A**), WT+LPS vs.
981 WT+PBS (**B**), *Sh3*$^{+/-}$+LPS vs. WT+LPS (**C**), *Sh3*$^{+/-}$+PBS vs. WT+PBS (**D**). Upregulated
982 genes are indicated in red color, downregulated genes are indicated in blue color and
983 DEGs below threshold are indicated in grey color.

984 **E-F. Venn diagrams show shared upregulated and downregulated genes among**
985 **four comparisons.** Shared upregulated (**E**) and downregulated genes (**F**) numbers are
986 shown within the diagrams. Comparison of *Sh3*$^{+/-}$+LPS vs *Sh3*$^{+/-}$+PBS is red diagram,
987 WT+LPS vs. WT+PBS is blue diagram, *Sh3*$^{+/-}$+LPS vs. WT+LPS is green diagram, and
988 *Sh3*$^{+/-}$+PBS vs. WT+PBS is yellow diagram.

989 **G. Bubble chart shows functions of DEGs of *Sh3*$^{+/-}$+LPS vs. WT+LPS comparison.**
990 Volcano plot of the negative log of p-value (Y-axis) vs. the z-score (X-axis). *p*-value was
991 calculated using the right-tailed Fisher's Exact Test. A negative log of p-value cutoff of
992 1.3 ($p < 0.05$) was used to identify significantly changed functional pathways. A z-score
993 range cutoff of ±0.1 was used to identify the activation or inhibition state of a canonical
994 pathway. Some names of pathways are annotated in the chart. Activated pathways are
995 orange bubbles and inhibited pathways are blue bubbles. The size of the bubbles reflects
996 the number of genes overlapped with the pathway database.

997 **Figure 4. Neuroinflammation increased in *Sh3*$^{+/-}$ mice compared to WT mice in**
998 **response to LPS.**

999 **A-D. Differential expression of neuroinflammatory marker genes *Il1b*, *Cxcl10,***
1000 ***Cx3cr1* and *P2ry12*.** At 24 hours after LPS injection, forebrain RNA was extracted, and
1001 RT-qPCR was performed. Target gene expression was normalized to the expression of
1002 the housekeeping gene GAPDH. One-way ANOVA was performed to compare gene
1003 expression in four groups (*Il1b*: F= 14.93, p = 0.0004, *Cxcl10*: F= 16.73, p = 0.0002,
1004 *Cx3cr1*: F= 14.8, p < 0.0001, *P2ry12*: F= 8.442, p = 0.0002). As expected, compared to
1005 PBS treatment, LPS significantly increased expression of *Il1b, Cxcl10*, and *Cx3cr1*, and
1006 decreased expression of *P2ry12* in both WT and *Sh3*$^{+/-}$ mice (*Il1b*: WT+PBS (n=10) vs.
1007 WT+LPS (n=9), p = 0.0005, *Cxcl10*: WT+PBS (n=10) vs. WT+LPS (n=6), p = 0.0105,
1008 *Cx3cr1*: WT+PBS (n=10) vs. WT+LPS (n=9), p = 0.0388, *P2ry12*: WT+PBS (n=10) vs.
1009 WT+LPS (n=8), p = 0.0241; *Il1b*: *Sh3*$^{+/-}$ +PBS (n=12) vs. *Sh3*$^{+/-}$ +LPS (n=11), p = 0.002,
1010 *Cxcl10*: *Sh3*$^{+/-}$ +PBS (n=12) vs. *Sh3*$^{+/-}$ +LPS (n=11), p = 0.0015, *Cx3cr1*: *Sh3*$^{+/-}$ +PBS
1011 (n=12) vs. *Sh3*$^{+/-}$ +LPS (n=12), p < 0.0001, *P2ry12*: *Sh3*$^{+/-}$ +PBS (n=11) vs. *Sh3*$^{+/-}$ +LPS
1012 (n=11), p = 0.0046). Significant increase of *Il1b, Cxcl10*, *Cx3cr1* was observed in *Sh3*$^{+/-}$
1013 +LPS vs. WT+LPS (*Il1b*: p = 0.0166, *Cxcl10*: p = 0.0076, *Cx3cr1*: p = 0.0004). In contrast,
1014 significantly increased expression of *P2ry12* was observed in *Sh3*$^{+/-}$+PBS vs. WT+PBS
1015 (p = 0.0102) and *Sh3*$^{+/-}$+LPS vs. WT+LPS (p = 0.036).

1016 **E-F. Increased immunohistochemistry fluorescence intensity of IBA1 in *Sh3*$^{+/-}$ +LPS**
1017 **group.** Mouse brain slices were collected at 3 hours and 24 hours after injection,
1018 respectively. Microglia activation was labeled with IBA1 antibody (**E1-E4, F1-F4**).
1019 Quantitative fluorescence intensity of IBA1 at cortex regions from WT+LPS, *Sh3*$^{+/-}$+PBS,

1020 and *Sh3*$^{+/-}$+LPS groups were normalized to WT+PBS group and then compared (Kruskal-
1021 Wallis test, **E5.** p = 0.0002; **F5.** p < 0.0001). LPS increased microglia activation in both
1022 WT and *Sh3*$^{+/-}$ mice at both 3 hours and 24 hours after injection compared to PBS groups
1023 (3 hours: WT+PBS (n=10) vs. WT+LPS (n=13), p = 0.0067, *Sh3*$^{+/-}$ +PBS (n=12) vs. *Sh3*$^{+/-}$
1024 +LPS (n=11), p = 0.0004. 24 hours: WT+PBS (n=9) vs. WT+LPS (n=16), p = 0.0053,
1025 *Sh3*$^{+/-}$ +PBS (n=15) vs. *Sh3*$^{+/-}$ +LPS (n=12), p < 0.0001). Moreover, LPS induced
1026 significant overactivation of microglia in *Sh3*$^{+/-}$ mice at 24 hours after injection compared
1027 to WT mice, not 3 hours (WT+LPS vs. *Sh3*$^{+/-}$ +LPS, 3 hours, p = 0.6204, 24 hours, p =
1028 0.0017).

1029 **G-I. Increased TLR4 and decreased SHANK3 protein expression in S*h3*$^{+/-}$ mice.** LPS
1030 receptor TLR4 and SHANK3 expression were examined in whole-cell lysates using
1031 western blot at 24 hours after injection. Target protein expression was normalized to β-
1032 ACTIN expression (**G**). Quantitative protein expression from WT+LPS, *Sh3*$^{+/-}$+PBS, and
1033 *Sh3*$^{+/-}$+LPS were normalized to WT+PBS group and one-way ANOVA was performed
1034 (TLR4, F = 14.38, p = 0.0001, SHANK3, F = 7.681, p = 0.0033). Significantly elevated
1035 TLR4 expression was observed in *Sh3*$^{+/-}$ mice compared to WT mice (**H**, WT+PBS vs.
1036 *Sh3*$^{+/-}$ +PBS, p < 0.0001; WT+LPS vs. *Sh3*$^{+/-}$ +LPS, p = 0.0081). As expected, significantly
1037 reduced SHANK3 expression was detected in *Sh3*$^{+/-}$ mice (**I**, WT+PBS vs. *Sh3*$^{+/-}$ +PBS,
1038 p = 0.0172; WT+LPS vs. *Sh3*$^{+/-}$ +LPS, p = 0.002).

1039 **J-P. Colocalization analysis of TLR4/IBA1 between WT+LPS vs. *Sh3*$^{+/-}$ +LPS group.**
1040 Mouse brain slices were collected at 24 hours after LPS injection in WT and *Sh3*$^{+/-}$ mice.
1041 IBA1 and TLR4 antibody were used for immunocytochemistry. Colocalization of IBA1 and
1042 TLR4 at cortex regions were analyzed and compared (**J-K**). Unpaired t-test was

1043 conducted. No difference in colocalization Pearson's coefficient between WT+LPS vs.
1044 *Sh3*$^{+/-}$ +LPS was observed (**L**, two-tailed $p = 0.2309$). *Sh3*$^{+/-}$ showed smaller normalized
1045 colocalization by TLR4 (**M**, two-tailed $p = 0.0093$) but similar normalized colocalization by
1046 IBA1 (**N**, two-tailed $p = 0.9141$) compared to WT. *Sh3*$^{+/-}$ showed decreased TLR4 cellular
1047 fluorescence intensity (**O**, two-tailed $p = 0.0183$) but increased IBA1 cellular fluorescence
1048 intensity (**P**, two-tailed $p = 0.0001$) than WT. * $p < 0.05$, ** $p < 0.005$, *** $p < 0.0005$, **** $p <$
1049 0.0001.

1050 **Figure 5. Microglia activation disrupted synaptic structure in *Sh3*$^{+/-}$ mice compared**
1051 **to WT mice in response to LPS.**

1052 **A-D. Increased vGluT1 engulfment in *Sh3*$^{+/-}$ mice at 24 hours after LPS injection. A.**
1053 Representative images of maximum projection of z-stack imaging of IBA1/CD68/vGluT1
1054 co-staining (left), 3D rendering masked by IBA1 and CD68 (center), and enlarged images
1055 of 3D rendering (right). Total volumes of masked vGluT1 and CD68 were calculated and
1056 unpaired t-test was conducted. No significant difference of IBA1 masked CD68
1057 occupancy was detected (**B.** two-tailed p = 0.7149). IBA1 and CD68 double masked
1058 vGluT1 occupancy and IBA1 masked vGluT1 occupancy was higher in *Sh3*$^{+/-}$ mice than
1059 WT mice (**C.** two-tailed $p < 0.0001$, **D.** two-tailed p = 0.0003).

1060 **E-H. Reduced synapses in *Sh3*$^{+/-}$ mice at 24 hours after LPS injection. E.**
1061 Representative images of super-resolution imaging of vGluT1/PSD95 co-staining at 24
1062 hours post-injection. Colocalized puncta of vGluT1and PSD95 were indicated by
1063 arrowheads and were counted as synapse puncta. Non-colocalized puncta of PSD95
1064 were indicated by arrows. Colocalization of vGluT1and PSD95 was analyzed, and
1065 number of colocalized puncta were counted as synapse density. Unpaired t-test was
1066 conducted. *Sh3*$^{+/-}$ mice showed a lower colocalization Pearson's coefficient (**F**, two-tailed
1067 p = 0.0002), a reduced normalized colocalization coefficient by PSD95 (**G**, two-tailed p =
1068 0.0056) and decreased synapse density (**H**, two-tailed p = 0.0107) compared to WT mice.

1069 **I-M. Reduced synapses in *Sh3*$^{+/-}$ mice at 2 weeks after LPS injection. I-J.**
1070 Representative images of super-resolution imaging of vGluT1/PSD95 co-staining at 2
1071 weeks post-injection among four groups, WT+PBS, WT+LPS, *Sh3*$^{+/-}$+PBS, and *Sh3*$^{+/-}$
1072 +LPS. Mask was generated based on the colocalized puncta of vGluT1and PSD95. Non-

1073 colocalized puncta of PSD95 were indicated by arrows in **J**. One-way ANOVA was
1074 conducted for comparing colocalization Pearson's coefficient (**K.** F = 4.254, p = 0.0088),
1075 colocalization coefficient by PSD95 (**L.** F = 26.51, p < 0.0001), and synapse density (**M.**
1076 F = 10.94, p < 0.0001). *Sh3*$^{+/-}$+LPS group showed a lower colocalization Pearson's
1077 coefficient than WT+LPS (p = 0.0067) or *Sh3*$^{+/-}$+PBS groups (p = 0.0022), a reduced
1078 normalized colocalization coefficient by PSD95 than WT+LPS (p < 0.0001) or *Sh3*$^{+/-}$+PBS
1079 groups (p < 0.0001) , and decreased synapse density than WT+LPS (p < 0.0001) or *Sh3*$^{+/-}$
1080 +PBS groups (p < 0.0001).

1081 **N-S. Reduced PSD95, HOMER 1b/c, NR2A and GluA1 expression in *Sh3*$^{+/-}$ mice at 2**
1082 **weeks after LPS injection.** Postsynaptic scaffold proteins PSD95 and HOMER 1b/c (**N**),
1083 and excitatory receptors NMDA subunit NR2A and AMPA subunit GluA1 expression (**Q**)
1084 were examined in forebrain PSD fractions using western blot at 2 weeks after injection.
1085 Target protein expression was normalized to β-ACTIN expression. Quantitative protein
1086 expression from WT+LPS, *Sh3*$^{+/-}$+PBS, and *Sh3*$^{+/-}$+LPS were normalized to WT+PBS
1087 group and one-way ANOVA was conducted (PSD95, F = 4.763, p = 0.006, HOMER 1b/c,
1088 F = 12.28, p < 0.0001, NR2A, F = 5.06, p = 0.0091, GluA1, F = 4.951, p = 0.0313). **O.**
1089 Significantly decreased PSD95 expression was detected in *Sh3*$^{+/-}$ mice not WT mice after
1090 LPS treatment (*Sh3*$^{+/-}$+LPS (n=11) vs. WT+LPS (n=12), p = 0.0009; *Sh3*$^{+/-}$+LPS (n=11)
1091 vs. *Sh3*$^{+/-}$+PBS (n=11), p = 0.0354). No significant change in PSD95 was detected
1092 between WT+PBS (n=12) vs. WT+LPS (p = 0.5153) or WT+PBS vs. *Sh3*$^{+/-}$+PBS (p =
1093 0.4845). **P.** Significantly reduced HOMER 1b/c expression was observed in *Sh3*$^{+/-}$ mice
1094 compared to WT mice (WT+PBS (n=6) vs. *Sh3*$^{+/-}$ +PBS (n=6), p < 0.0001; WT+LPS (n=6)
1095 vs. *Sh3*$^{+/-}$+LPS (n=6), p = 0.0088). No significant change of HOMER 1b/c was detected

1096 after LPS treatment (WT+PBS vs. WT+LPS (p = 0.1781) or *Sh3*$^{+/-}$+PBS vs. *Sh3*$^{+/-}$+LPS
1097 (p = 0.318)). **R.** *Sh3*$^{+/-}$+LPS group (n=6) showed significant decreased NR2A expression
1098 compared to both the *Sh3*$^{+/-}$+PBS group (n=6) (p = 0.0053) and the WT+LPS group (n=6)
1099 (p = 0.002). No significant change of NR2A was observed between WT+PBS (n=6) vs.
1100 WT+LPS (p = 0.1404) or WT+PBS vs. *Sh3*$^{+/-}$+PBS (p = 0.2827). **S.** *Sh3*$^{+/-}$+LPS group
1101 (n=3) showed significantly reduced GluA1 expression compared to both the *Sh3*$^{+/-}$ +PBS
1102 group (n=3) (p = 0.0378) and the WT+LPS group (n=3) (p = 0.0169). No significant
1103 change in GluA1 was found between WT+PBS (n=3) vs. WT+LPS (p = 0.5898) or
1104 WT+PBS vs. *Sh3*$^{+/-}$+PBS (p = 0.3102). * $p < 0.05$, ** $p < 0.005$, *** $p < 0.0005$, **** $p < 0.0001$.

1105

1106 **Figure 6. Summary of increased neuroinflammation susceptibility in *Sh3*$^{+/-}$ mice.**

1107 The schematic drawing proposes a model of increased neuroinflammation and altered
1108 behavioral phenotypes in *Shank3* haploinsufficiency mouse after LPS treatment.

1109 Generally speaking, LPS evokes neuroinflammation through three distinct pathways, 1)
1110 LPS binds to TLR4 expressed on neutrophils, promoting neutrophil infiltration through
1111 blood-brain barrier and activation of microglia cells; 2) LPS binds to TLR4 expressed in
1112 cerebral endothelial cells located in blood-brain barrier, compromising the integrity of
1113 blood-brain barrier and increasing permeability of additional immune components
1114 entering the brain; 3) LPS that penetrates blood-brain barrier binds to TLR4 expressed in
1115 microglia, activating microglia and triggering proinflammatory cytokines release. In *Sh3*$^{+/-}$
1116 brain vs. WT brain, we observed excessive proinflammatory gene expression,
1117 proinflammatory cytokines, overactivation of microglia and increased expression of TLR4
1118 at 24 hours after LPS injection. It suggests that LPS might exacerbate neuroinflammation
1119 responses through above routes in *Sh3*$^{+/-}$ mice.

1120 Microglia activation can sculpt synapses and brain circuits and change animal behavioral
1121 phenotypes long-term. In *Sh3*$^{+/-}$ brain vs. WT brain, we observed elevated microglia
1122 engulfment, reduced synapse, and decreased synaptic transmission gene expression at
1123 24 hours after LPS injection, suggesting increased synapse elimination in *Sh3*$^{+/-}$ mice. At
1124 2 weeks after LPS injection, we observed reduced synapse density, decreased PSD95
1125 expression and lower expression of excitatory receptor expression. It indicates that
1126 neuroinflammation-induced synaptic dysfunction was associated with behavioral changes
1127 found in *Sh3*$^{+/-}$ mice.

Figure 1

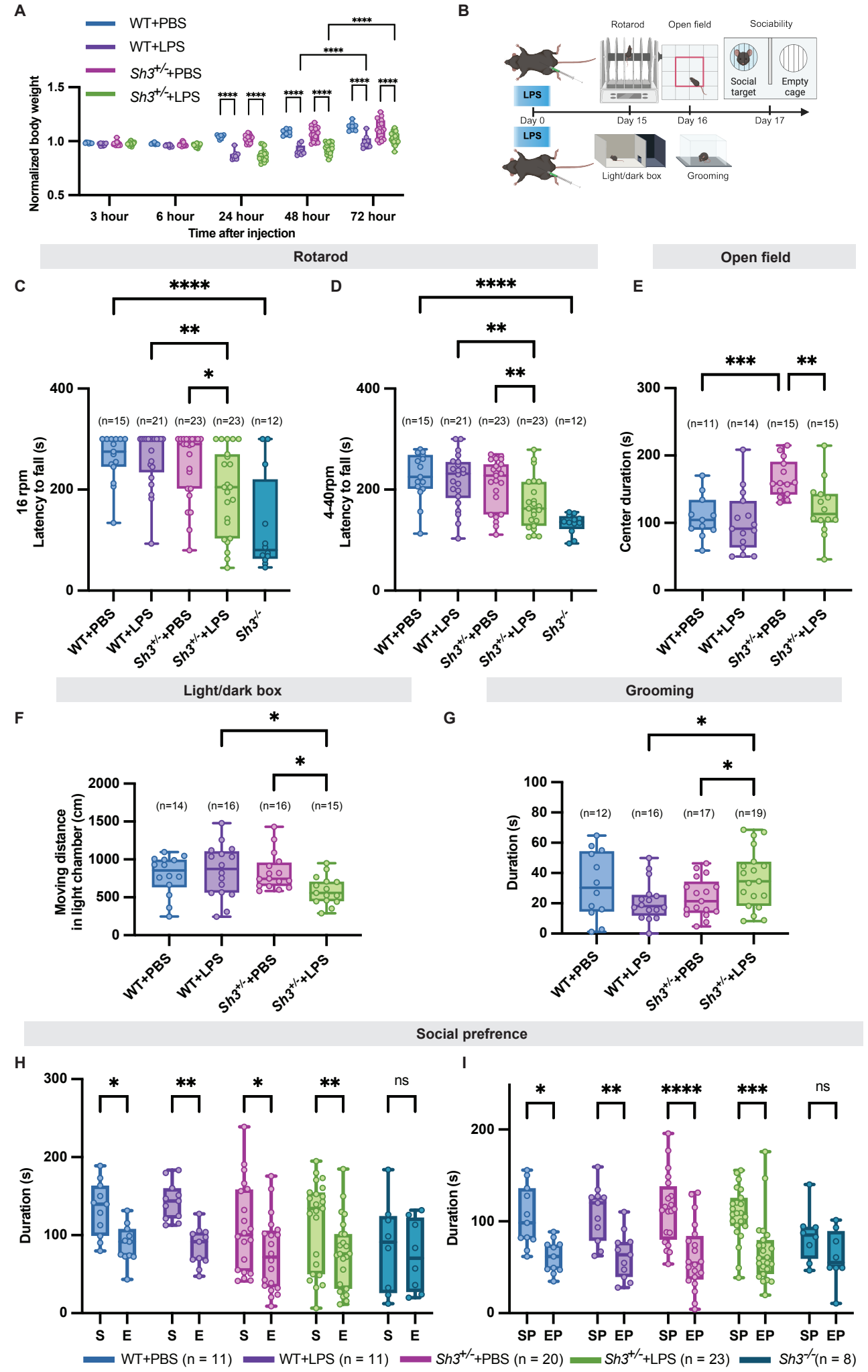
A
WT+PBS
WT+LPS
Sh3+/-+PBS
Sh3+/-+LPS
Normalized body weight
1.5
1.0
0.5
3 hour
6 hour
24 hour
48 hour
72 hour
Time after injection
B
Rotarod
Open field
Sociability
Social target
Empty cage
LPS
Day 0
Day 15
Day 16
Day 17
Light/dark box
Grooming
Rotarod
Open field
C
16 rpm Latency to fall (s)
(n=15) (n=21) (n=23) (n=23) (n=12)
D
4-40rpm Latency to fall (s)
(n=15) (n=21) (n=23) (n=23) (n=12)
E
Center duration (s)
(n=11) (n=14) (n=15) (n=15)
WT+PBS
WT+LPS
Sh3+/-+PBS
Sh3+/-+LPS
Sh3-/-
Light/dark box
Grooming
F
Moving distance in light chamber (cm)
(n=14) (n=16) (n=16) (n=15)
G
Duration (s)
(n=12) (n=16) (n=17) (n=19)
Social prefrence
H
Duration (s)
S E S E S E S E S E
I
Duration (s)
SP EP SP EP SP EP SP EP SP EP
WT+PBS (n = 11)
WT+LPS (n = 11)
Sh3+/-+PBS (n = 20)
Sh3+/-+LPS (n = 23)
Sh3-/-(n = 8)

Figure 2

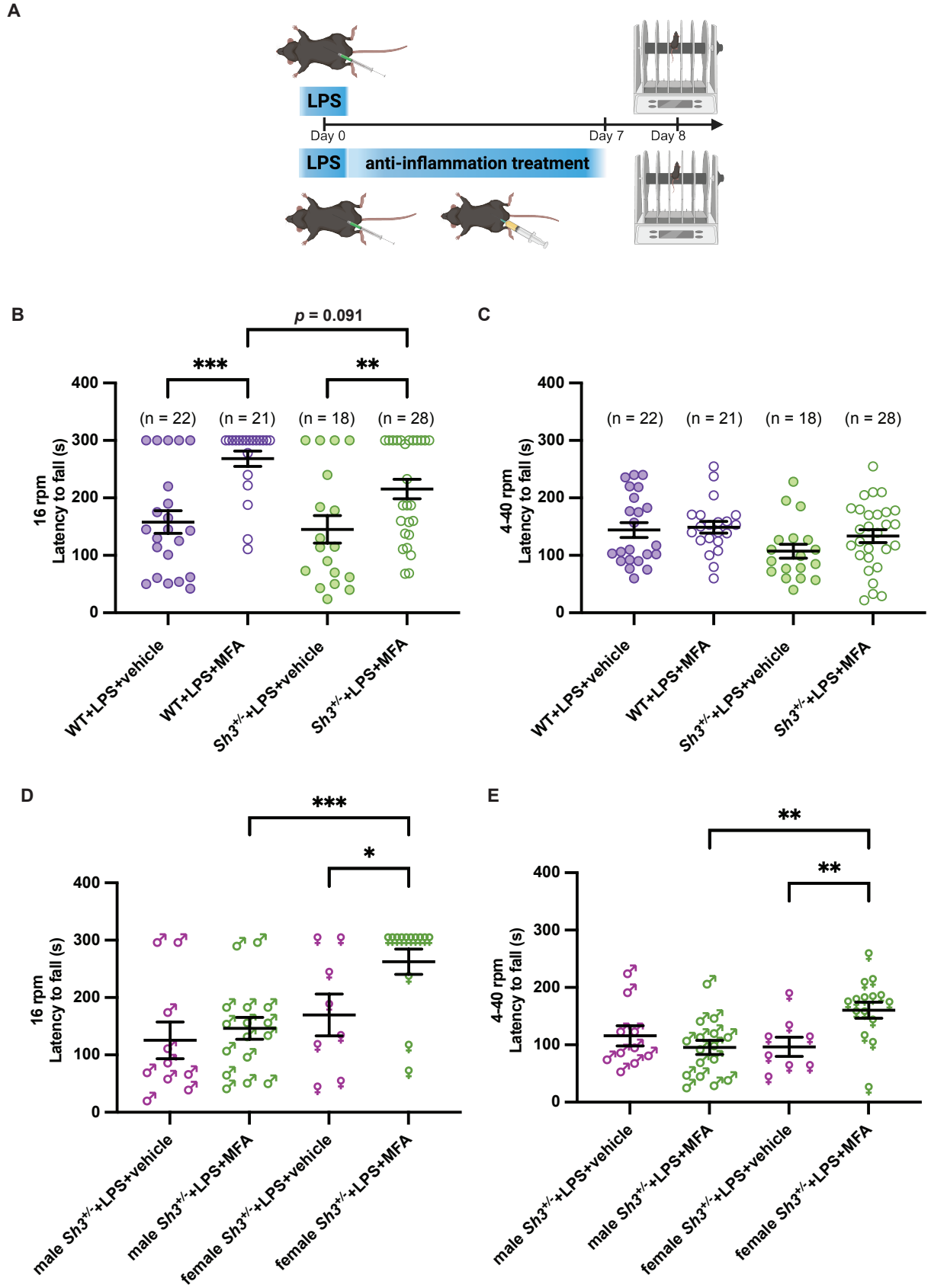
A
LPS
Day 0
Day 7
Day 8
LPS
anti-inflammation treatment
B
p = 0.091
***
**
(n = 22)
(n = 21)
(n = 18)
(n = 28)
16 rpm
Latency to fall (s)
400
300
200
100
0
WT+LPS+vehicle
WT+LPS+MFA
Sh3+/-+LPS+vehicle
Sh3+/-+LPS+MFA
C
(n = 22)
(n = 21)
(n = 18)
(n = 28)
4-40 rpm
Latency to fall (s)
400
300
200
100
0
WT+LPS+vehicle
WT+LPS+MFA
Sh3+/-+LPS+vehicle
Sh3+/-+LPS+MFA
D
***
*
16 rpm
Latency to fall (s)
400
300
200
100
0
male Sh3+/-+LPS+vehicle
male Sh3+/-+LPS+MFA
female Sh3+/-+LPS+vehicle
female Sh3+/-+LPS+MFA
E
**
**
4-40 rpm
Latency to fall (s)
400
300
200
100
0
male Sh3+/-+LPS+vehicle
male Sh3+/-+LPS+MFA
female Sh3+/-+LPS+vehicle
female Sh3+/-+LPS+MFA

Figure 3

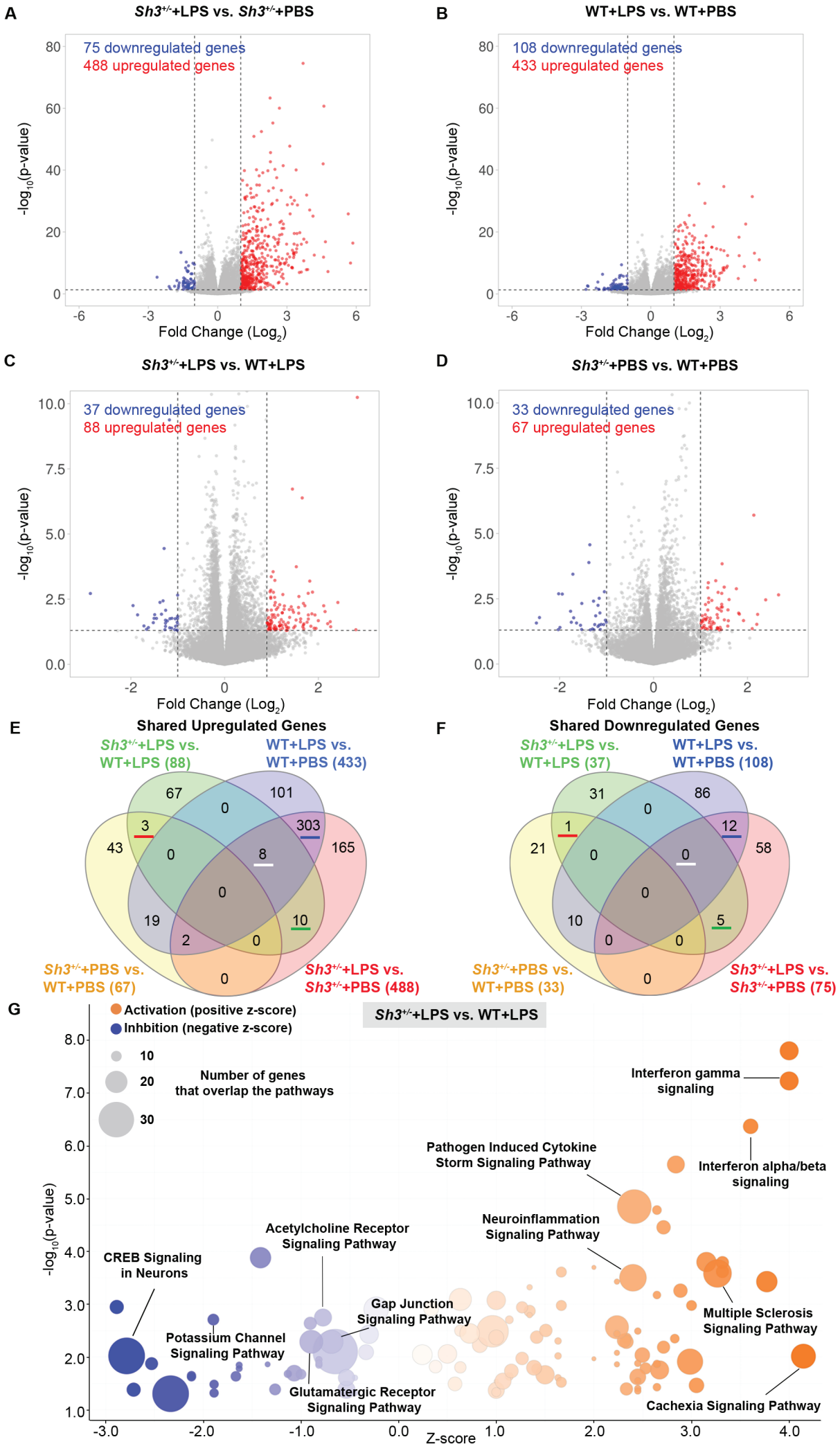
A
Sh3+/-+LPS vs. Sh3+/-+PBS
75 downregulated genes
488 upregulated genes
-log10(p-value)
Fold Change (Log2)
B
WT+LPS vs. WT+PBS
108 downregulated genes
433 upregulated genes
C
Sh3+/-+LPS vs. WT+LPS
37 downregulated genes
88 upregulated genes
D
Sh3+/-+PBS vs. WT+PBS
33 downregulated genes
67 upregulated genes
E
Shared Upregulated Genes
Sh3+/-+LPS vs. WT+LPS (88)
WT+LPS vs. WT+PBS (433)
Sh3+/-+PBS vs. WT+PBS (67)
Sh3+/-+LPS vs. Sh3+/-+PBS (488)
F
Shared Downregulated Genes
Sh3+/-+LPS vs. WT+LPS (37)
WT+LPS vs. WT+PBS (108)
Sh3+/-+PBS vs. WT+PBS (33)
Sh3+/-+LPS vs. Sh3+/-+PBS (75)
G
Sh3+/-+LPS vs. WT+LPS
Activation (positive z-score)
Inhbition (negative z-score)
Number of genes that overlap the pathways
Interferon gamma signaling
Interferon alpha/beta signaling
Pathogen Induced Cytokine Storm Signaling Pathway
Neuroinflammation Signaling Pathway
Acetylcholine Receptor Signaling Pathway
CREB Signaling in Neurons
Gap Junction Signaling Pathway
Multiple Sclerosis Signaling Pathway
Potassium Channel Signaling Pathway
Glutamatergic Receptor Signaling Pathway
Cachexia Signaling Pathway
Z-score

Figure 4

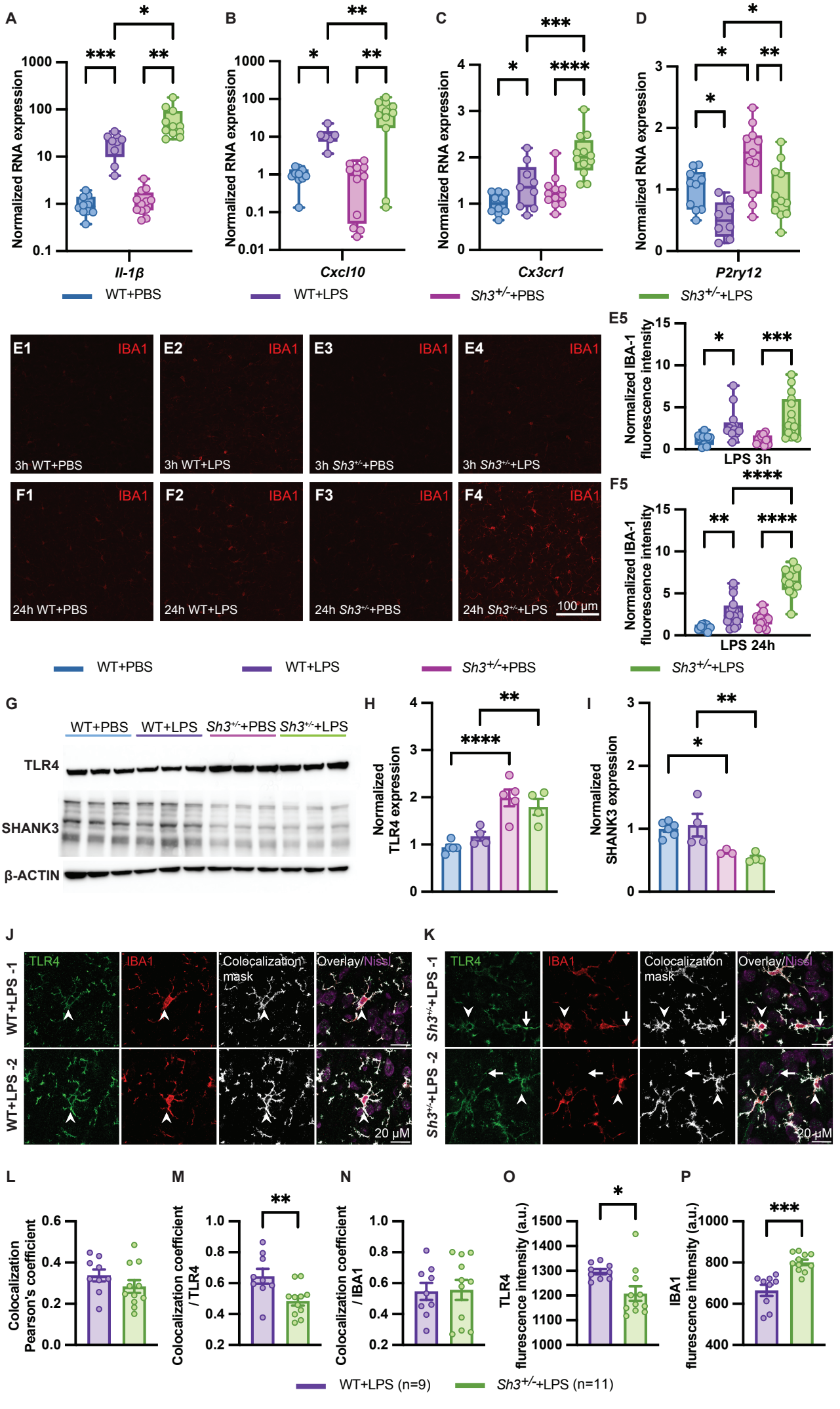
A
B
C
D
Normalized RNA expression
Il-1β
Cxcl10
Cx3cr1
P2ry12
WT+PBS
WT+LPS
Sh3+/-+PBS
Sh3+/-+LPS
E1
E2
E3
E4
F1
F2
F3
F4
IBA1
3h WT+PBS
3h WT+LPS
3h Sh3+/-+PBS
3h Sh3+/-+LPS
24h WT+PBS
24h WT+LPS
24h Sh3+/-+PBS
24h Sh3+/-+LPS
100 µm
E5
F5
Normalized IBA-1 fluorescence intensity
LPS 3h
LPS 24h
G
WT+PBS
WT+LPS
Sh3+/-+PBS
Sh3+/-+LPS
TLR4
SHANK3
β-ACTIN
H
Normalized TLR4 expression
I
Normalized SHANK3 expression
J
K
WT+LPS -1
WT+LPS -2
Sh3+/-+LPS -1
Sh3+/-+LPS -2
TLR4
IBA1
Colocalization mask
Overlay/Nissl
20 µM
L
M
N
O
P
Colocalization Pearson's coefficient
Colocalization coefficient / TLR4
Colocalization coefficient / IBA1
TLR4 fluorescence intensity (a.u.)
IBA1 fluorescence intensity (a.u.)
WT+LPS (n=9)
Sh3+/-+LPS (n=11)

Figure 5

24 hours after LPS/PBS injection

A

B

C

D

E

F

G

H

2 weeks after LPS/PBS injection

I

J

K

L

M

N

Q

O

P

R

S

Figure 6

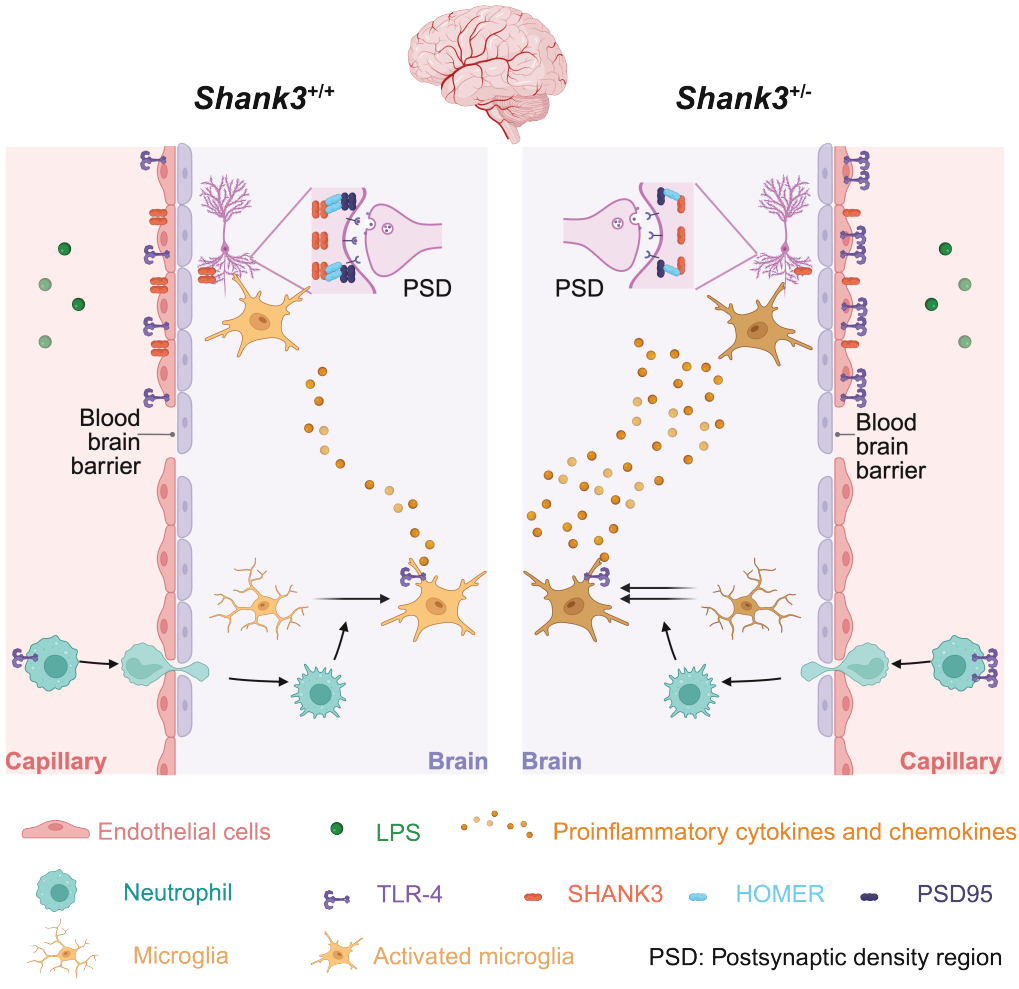
Shank3+/+
Shank3+/-
PSD
PSD
Blood brain barrier
Blood brain barrier
Capillary
Brain
Brain
Capillary
Endothelial cells
LPS
Proinflammatory cytokines and chemokines
Neutrophil
TLR-4
SHANK3
HOMER
PSD95
Microglia
Activated microglia
PSD: Postsynaptic density region